THE PROPER MOTION OF THE MAGELLANIC CLOUDS. I.
FIRST RESULTS AND DESCRIPTION OF THE PROGRAM

Edgardo Costa[1], René A. Méndez[1], Mario H. Pedreros[2], Maximiliano Moyano[1], Carme Gallart[3], Noelia Noël[3],
Gustavo Baume[4], and Giovanni Carraro[5]

[1] Departamento de Astronomía, Universidad de Chile, Casilla 36-D, Santiago, Chile; costa@das.uchile.cl, rmendez@das.uchile.cl, mmoyano@das.uchile.cl, mmoyano@mpia-hd.mpg.de
[2] Departamento de Física, Universidad de Tarapacá, Casilla 7-D, Arica, Chile; mpedrero@uta.cl
[3] Instituto de Astrofísica de Canarias, Tenerife 38200, Islas Canarias, Spain; carme@iac.es, noelia@iac.es
[4] Facultad de Ciencias Astronómicas y Geofísicas de la UNLP, IALP-CONICET, Paseo El Bosque s/n, La Plata, Argentina; gbaume@gmail.com
[5] European Southern Observatory, Alonso de Cordova 3107, Santiago, Chile; gcarraro@eso.org

ABSTRACT

We present the first results of a ground-based program to determine the proper motion of the Magellanic Clouds (MCs) relative to background quasars (QSO), being carried out using the Iréneé du Pont 2.5 m telescope at Las Campanas Observatory, Chile. Eleven QSO fields have been targeted in the Small Magellanic Cloud (SMC) over a time base of six years, and with seven epochs of observation. One quasar field was targeted in the Large Magellanic Cloud (LMC), over a time base of five years, and with six epochs of observation. The shorter time base in the case of the LMC is compensated by the much larger amount of high-quality astrometry frames that could be secured for the LMC quasar field (124 frames), compared to the SMC fields (an average of roughly 45 frames). In this paper, we present final results for field Q0557−6713 in the LMC and field Q0036−7227 in the SMC. From field Q0557−6713, we have obtained a measured proper motion of $\mu_{\alpha} \cos \delta = +1.95 \pm 0.13$ mas yr^{-1}, $\mu_{\delta} = +0.43 \pm 0.18$ mas yr^{-1} for the LMC. From field Q0036−7227, we have obtained a measured proper motion of $\mu_{\alpha} \cos\delta = +0.95 \pm 0.29$ mas yr^{-1}, $\mu_{\delta} = -1.14 \pm 0.18$ mas yr^{-1} for the SMC. Although we went through the full procedure for another SMC field (QJ0036−7225), on account of unsolvable astrometric difficulties caused by blending of the QSO image, it was impossible to derive a reliable proper motion. Current model rotation curves for the plane of the LMC indicate that the rotational velocity ($V_{\rm rot}$) at the position of LMC field Q0557−6713 can be as low as 50 km s^{-1}, or as high as 120 km s^{-1}. A correction for perspective and rotation effects leads to a center of mass proper motion for the LMC of $\mu_{\alpha} \cos\delta = +1.82 \pm 0.13$ mas yr^{-1}, $\mu_{\delta} = +0.39 \pm 0.15$ mas yr^{-1} ($V_{\rm rot} = 50$ km s^{-1}), and to $\mu_{\alpha} \cos\delta = +1.61 \pm 0.13$ mas yr^{-1}, $\mu_{\delta} = +0.60 \pm 0.15$ mas yr^{-1} ($V_{\rm rot} = 120$ km s^{-1}). Assuming that the SMC has a disk-like central structure, but that it does not rotate, we obtain a center of mass proper motion for the SMC of $\mu_{\alpha} \cos\delta = +1.03 \pm 0.29$ mas yr^{-1}, $\mu_{\delta} = -1.09 \pm 0.18$ mas yr^{-1}. Our results are in reasonable agreement with most previous determinations of the proper motion of the MCs, including recent *Hubble Space Telescope* measurements. Complemented with published values of the radial velocity of the centers of the LMC and SMC, we have used our proper motions to derive the galactocentric (gc) velocity components of the MCs. For the LMC, we obtain $V_{\rm gc,t} = +315 \pm 20$ km s^{-1}, $V_{\rm gc,r} = +86 \pm 17$ km s^{-1} ($V_{\rm rot} = 50$ km s^{-1}), and $V_{\rm gc,t} = +280 \pm 24$ km s^{-1}, $V_{\rm gc,r} = +94 \pm 17$ km s^{-1} ($V_{\rm rot} = 120$ km s^{-1}). For the SMC, we obtain $V_{\rm gc,t} = +258 \pm 50$ km s^{-1}, $V_{\rm gc,r} = +20 \pm 44$ km s^{-1}. These velocities imply a relative velocity between the LMC and SMC of 84 ± 50 km s^{-1}, for $V_{\rm rot,LMC} = 50$ km s^{-1}, and 62 ± 63 km s^{-1} for $V_{\rm rot,LMC} = 120$ km s^{-1}. Albeit our large errors, these values are not inconsistent with the standard assumption that the MCs are gravitationally bound to each other.

Key words: astrometry – Local Group – Magellanic Clouds

Online-only material: color figures

1. INTRODUCTION

Studying the kinematics of the Local Group galaxies nearest to our Galaxy is critical to understanding the formation process of our Galaxy and that of its satellites. Topics such as the origin of stellar streams that seem to be related to these satellites, the role of tidal interactions in the evolution of low-mass galaxies and of the halo of our Galaxy, and, in general, the origin of these minor groups, could be better addressed having a precise knowledge of the orbits of these satellites.

Among the objects that can help understand the topics outlined above are the Magellanic Clouds (MCs), whose structures and kinematics show various evidences of mutual interaction, and interaction with the Milky Way (MW). Additionally, on account of being among the closest galaxies to the MW, they are the most suitable for kinematical studies with present ground-based astrometric techniques. All attempts to model the space motions of the MCs require a precise knowledge of their present space velocity vectors, a major task given the difficulty of measuring their proper motions in order to determine their transverse velocities (in contrast, their radial velocities are well established).

The earliest efforts to measure the proper motions of the MCs are those of Kroupa et al. (1994), who obtained preliminary proper motions with respect to the PPM catalog (Röser & Bastian 1993); Jones et al. (1994), who used photographic plates to measure the proper motion of the Large Magellanic Cloud (LMC) with respect to background galaxies; and Kroupa & Bastian (1997), who used *Hipparcos* (ESA 1997) data to determine the proper motion of both clouds. Save for the work of Momany & Zaggia (2005, hereafter MZ05), who used UCAC2

(Zacharias et al. 2004) data to determine the proper motion of both clouds, in the last decade, the proper motion of the MCs has been measured with respect to background QSOs. Results from ground-based observations, specifically for the LMC, are those of Anguita et al. (2000, hereafter ALP00), Drake et al. (2001), Pedreros et al. (2002, hereafter PAM02; 2006, hereafter PCM06). With the exception of the results by ALP00 and MZ05, all the above results for the LMC are consistent within the declared errors. The results by ALP00 and MZ05, pointing to the MCs being unbound to the MW, are currently considered to be affected by systematic errors (see below). More recently, high internal precision proper motions for both clouds have resulted from *Hubble Space Telescope* (*HST*) observations, namely those of Kallivayalil et al. (2006a, 2006b; hereafter K06a and K06b, respectively) and Piatek et al. (2008, hereafter PI08). We present data from these studies later in Tables 7 and 8.

In parallel to the observational effort, various models for the MW–LMC–SMC system have been proposed, looking for Magellanic orbits that best reproduce conspicuous features of the Magellanic system which are believed to be the result of dynamical interactions of this triple system. The most notable of these are the Magellanic Stream (MS), the intercloud bridge, and the common gas envelope. Precise knowledge of the orbits of the MCs is also required to determine if the MCs are gravitationally bound to each other, and to determine if they are bound to the MW. The first detailed analysis of the interactions is probably that of Murai & Fujimoto (1980), who modeled the motion of the MCs in a massive galactic halo, and found that the Magellanic orbits that best reproduced the MS and the intercloud bridge required that the MCs have been gravitationally bound to each other for the past 10^{10} years. Their (model) Stream is the result of tidal stripping of the Small Magellanic Cloud (SMC) due to a close encounter with the LMC. Gardiner et al. (1994) used this same numerical model with revised observational parameters and different initial constraints, and reached similar conclusions. A brief review of these and related models can be found in Kroupa et al. (1994) and in Lin et al. (1995). A more elaborate version of this scheme is presented in Gardiner & Noguchi (1996, hereafter GN96), who confirmed their previous findings and added many details to the interpretation of the morphology of the MS. The above models fall in the category of "Tidal Interaction" models, given that they invoke tidal interactions between the MW–LMC–SMC system to explain the formation of the MS. Several criticisms have added against the tidal models (see, e.g., Gingold 1984; Moore & Davis 1994), the most obvious of which is, perhaps, that the Stream is purely gaseous and there is no clear evidence of stars in it (if the MS is purely of tidal origin, stars should have been stripped as easily as gas).

Another main category of models to explain the formation of the MS are the "Ram Pressure Stripping" models. In these models the MS is not formed directly by tidal interactions between the MCs and the MW, but caused by hydrodynamic effects. According to these models, the onset of the formation of the MS was also a collision between the LMC and the SMC, which first formed the intercloud region. The MS was later formed from this region via interactions between MC gas with Galactic hydrogen ("Diffuse Ram Pressure"; see, e.g., Meurer et al. 1985; Moore & Davis 1994; Heller & Rohlfs 1994; Mastropietro et al. 2005), or with high-velocity Galactic Halo gas clouds ("Discrete Ram Pressure"; see, e.g., Mathewson et al. 1987; Wayte 1991). Ram models are not free of problems, the most notorious being their difficulty to reproduce the leading

counterpart to the MS (the Leading Arm). As discussed by Yoshizawa & Noguchi (2003) and Connors et al. (2006), most recent theoretical work seems to favor tidal models. This matter is, however, far from being settled. Recent models by Besla et al. (2007), using observational parameters from K06a and K06b, indicate that all previously proposed mechanisms for explaining the origin of the MS may need to be revisited.

To elucidate these matters, additional physics is needed on the one hand to more quantitatively model the observed properties of the MS and other features of the Magellanic system, and on the other hand it is necessary to improve the precision of the space velocity vectors of the MCs to better constrain the models. As mentioned before, this latter requirement currently resumes the task of precisely measuring the proper motions of the MCs in order to determine their transverse velocities, which is the motivation of the present research.

At the time our program was conceived ($\sim$2000), the observational effort had concentrated on the LMC, and the preliminary results of Kroupa et al. (1994) and Kroupa & Bastian (1997) were the only published values for the proper motion of the SMC. Another (higher precision) work by Irwin et al. (1996) based on photographic plates was never published, and their results were just quoted in Irwin (1999). This motivated us to start a program in 2001 to measure proper motion of the SMC with respect to 11 QSOs in its background.

Given that previous theoretical/observational research indicated that the total expected proper motion of the SMC should be about 1.5 mas yr^{-1}, a conservative proper motion precision of $\sim$0.5 mas yr^{-1} (per QSO), to be achieved on a time base of six years, and with seven epochs of observation, was deemed sufficient to address our goal (in the end we were able to achieve a higher precision; see Tables 7 and 8). Based on previous astrometric experience by Costa & Loyola (1999) with the Irénée du Pont 2.5 m telescope (C100) at Las Campanas Observatory (LCO), Chile, this instrument was chosen as the smallest telescope with which our program was feasible.

To check for consistency, one of the LMC background QSOs used by ALP00 and PCM06 (Q0557$-$6713) to determine the proper motion of the LMC was included in our program. A very large number of frames could be obtained for this field, leading to a high precision determination of the proper motion of the LMC. Again at the time our program was started, an additional motivation for these observations was to solve the puzzling discrepancy between the proper motion in declination determined by ALP00 and those determined previously, as well as with that determined by PAM02. This issue was, however, recently addressed by PCM06, who seem to have clarified the problem. PCM06 used essentially the same observational setup and reduction procedure used by ALP00, and also included unmodified pixel coordinates (see Section 3.2) from ALP00 to obtain their proper motion for the LMC; yet, their result agrees well with measurements by other groups. This lead PCM06 to conclude that ALP00's discrepant declination proper motion originated in their final processing steps. See PCM06 for details.

The SMC background QSOs were selected from the works of Tinney et al. (1997) and Tinney (1999), who provide lists of spectroscopically confirmed QSOs behind the nearest MW satellite galaxies. Based on the appearance of their optical images in our CCD frames, of the 11 QSOs presented in these works 10 of them seemed adequate for astrometry. They have B magnitudes in the range $\sim$19–20. The LMC background QSO was identified by Blanco & Heathcote (1986), and has $B \sim 17$. In Table 1, we list the identification and coordinates of all
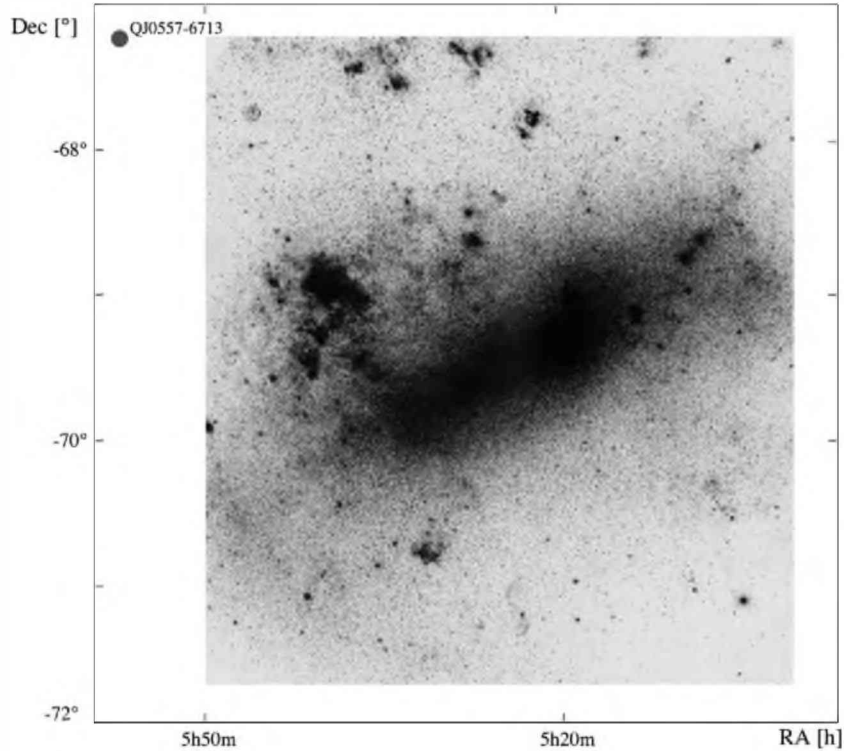
Figure 1. *R*-band image of the LMC schematically showing the location of the background quasar QJ0557−6713. The image is roughly $4.5 \times 5°$. North is at the top and east to the left. LMC image courtesy of Cerro El Roble Astronomical Station, Chile.

Table 1
Quasars Targeted in the Background of the MCs

QSO	R.A. (J2000.0)	Decl. (J2000.0)	Galaxy
QJ0557−6713	05 57 18.2	−67 13 22	LMC
QJ0033−7028	00 33 55.7	−70 29 00	SMC
QJ0033−7546	00 33 49.4	−75 46 24	SMC
QJ0035−7201	00 35 29.7	−72 01 23	SMC
QJ0036−7225	00 36 31.5	−72 25 38	SMC
QJ0036−7227	00 36 39.7	−72 27 42	SMC
QJ0037−7218	00 37 20.0	−72 18 00	SMC
QJ0047−7530	00 47 40.8	−75 30 10	SMC
QJ0102−7546	01 02 18.3	−75 46 49	SMC
QJ0111−7249	01 11 41.7	−72 49 47	SMC
QJ0112−7236	01 12 49.5	−72 36 10	SMC
QJ0116−7259	01 16 33.4	−72 59 49	SMC

MC background QSOs targeted in the present program, and in Figures 1 and 2, we illustrate schematically the position of our QSO fields, relative to the main body of both galaxies.

In this paper, we present final results for field Q0557−6713 in the LMC, and field Q0036−7227 in the SMC. As discussed in Section 3.7, we also went through the full reduction procedure for another SMC field (QJ0036−7225), but, because of unsolvable astrometric difficulties (blending of the QSO image), it was impossible to derive a reliable proper motion. This QSO field will be ignored in what follows. On account of the very large number of frames available for Q0557−6713, it was possible to determine a proper motion for the LMC with only six epochs of observation in a time base of five years; which was quite useful given its role as control field. Of the 10 SMC background QSOs targeted, we have at present enough data to determine final results only for the two QSOs mentioned above; we expect to obtain a final epoch for the rest in 2008/2009. This is not the result of chance: throughout our program these two SMC

fields were privileged because, being among the closest of our sample to the main body of the SMC, they are the less likely to be affected by chaotic motion known to be present in the outskirts of the SMC, in particular in its eastern side (Irwin et al. 1996). In Table 2, we summarize the observational material acquired for the QSO fields for which results are reported in this paper.

The astrometric program described here is part of a more comprehensive study of the SMC–LMC–MW system, which includes determining the star formation history (SFH) of the MCs via comparison of color–magnitude diagrams (CMDs) of MC fields with synthetic CMDs (see Noël et al. 2007; N. Noël et al. 2009, in preparation). This study should lead to a greater understanding of the evolution of the Magellanic system, and provide insights about the role of the interactions between the MCs and the MW in stimulating star formation in the MCs, and on the formation of the Galactic halo.

2. OBSERVATIONS AND CALIBRATIONS

All observations were carried out with a Tektronic CCD detector (Tek 5) attached to the Cassegrain focus of the C100 telescope at LCO. This 2048×2048 pixel^2 CCD is backside illuminated, thinned, and has 24 μm pixels. The CCD was operated without binning, at a gain of 3 e^-/ADU, implying a readout noise of 7 e^-. We note that this chip has a saturation level (in e^-) above the digital 32,767 ADU saturation level, so the observations are limited by the ADC converter, and not by its full well capacity. QE and other detector characteristics can be found at http://dornoch.lco.cl:8080/lco/telescopes-information/irenee-du-pont/instruments/specs/du-pont-telescope-direct-ccd-camera-ccd. Given the C100 focal ratio of $f/7.5$, this setup provides direct imaging over a field of $\sim 8.85 \times 8.85$, with a scale of ~ 0.26 arcsec pixel^{-1} (10.8 mm^{-1}).
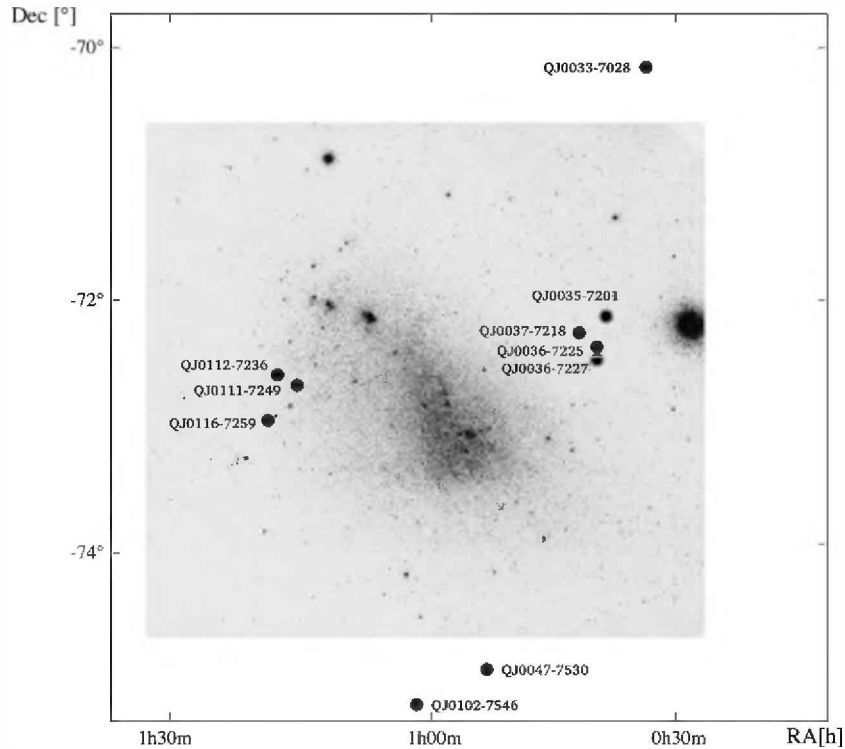
Figure 2. *R*-band image of the SMC schematically showing the spatial distribution of our 10 SMC fields with background quasars. The image is roughly $5° \times 4°.5$. North is at the top and east to the left. SMC image courtesy of Cerro El Roble Astronomical Station, Chile.

Table 2
Observational Material

Field	Epochs	Astrometry Frames	Epoch Range	DCR Frames
QJ0557−6713—LMC	6	124	2001.79–2006.81	23
QJ0036−7227—SMC	7	42	2001.79–2007.78	17
QJ0036−7225—SMC[a]	7	46	2001.79–2007.78	18

Note. [a] Not used to determine the proper motion reported for the SMC (see the text).

To minimize the effects of refraction, all astrometric observations were carried out in the *R* bandpass. This was achieved using the LC-3010 red filter of the "Harris" *UBVRI* filter set. This set constitutes the default option on the C100 for broad-band photometry on the Johnson–Kron–Cousins system. Transmission curves can be found at: http://www.lco.cl/lco/telescopes-information/irenee-du-pont/instruments/website/direct-ccd-manuals/direct-ccd-manuals/3×3-filters-for-ccd-imaging. For similar reasons, the astrometric observations were restricted to hour angles less than ∼1.5 hr. In the case of the SMC, given the large number of background QSOs targeted (and the available telescope time), this latter condition restricted the number of astrometric frames that could be obtained for each QSO field to a maximum of nine (typically six) frames per epoch.

Although in the above conditions refraction effects are minor, to model the subtle effect of Differential Color Refraction (DCR) on the measured positions (see Section 3.4) special sets of additional observations were required: the "DCR Series." These series consist typically of 20 *sequential* images of each QSO field, with hour angles spanning from ∼0.5 hr to ∼3.5 hr from the meridian.

In order to reach a signal-to-noise ratio (S/N) of ∼150 over the full point-spread function (PSF) for the faintest objects of interest ($R \sim 20.5$), exposure times of ∼600 s were required for most of the QSOs in the background of the SMC, and

∼300–400 s for QJ0557−6713 in the background of the LMC. This S/N requirement comes from our original goal of achieving a proper motion precision of ∼0.5 mas yr^{-1} on a time base of six years, which in turn demanded a positional precision of ∼2 mas. Based on our experience with DAOPHOT (Stetson 1987), to measure the (X, Y) position of the centroids of stellar PSFs with such a precision requires an S/N ∼ 150. Prevailing good seeing conditions at LCO together with the fact that all observations were carried out in dark time, made it relatively easy to reach the desired S/N. We note that the frames used for the final astrometric solutions were taken with seeing conditions that varied between 0″.7 and 1″.3, with an average of ∼0″.9.

To reduce the effect of optical distortions on the relative position of the QSO and the local system of reference stars used to determine the proper motion, each QSO was placed in all corresponding frames within a few pixels of a certain position, which was selected on the first epoch of observations. This positioning strategy has the added benefit of ensuring that all reference stars are present in all images of a given QSO field.

The CCD frames were calibrated using standard IRAF[6] (ver. 2.11.3) tasks. For this purpose, Zero frames and Dome Flat frames were taken every night. Dark frames were also obtained

---

[6] IRAF is distributed by the National Optical Astronomy Observatories, which are operated by the Association of Universities for Research in Astronomy, Inc., under cooperative agreement with the National Science Foundation.
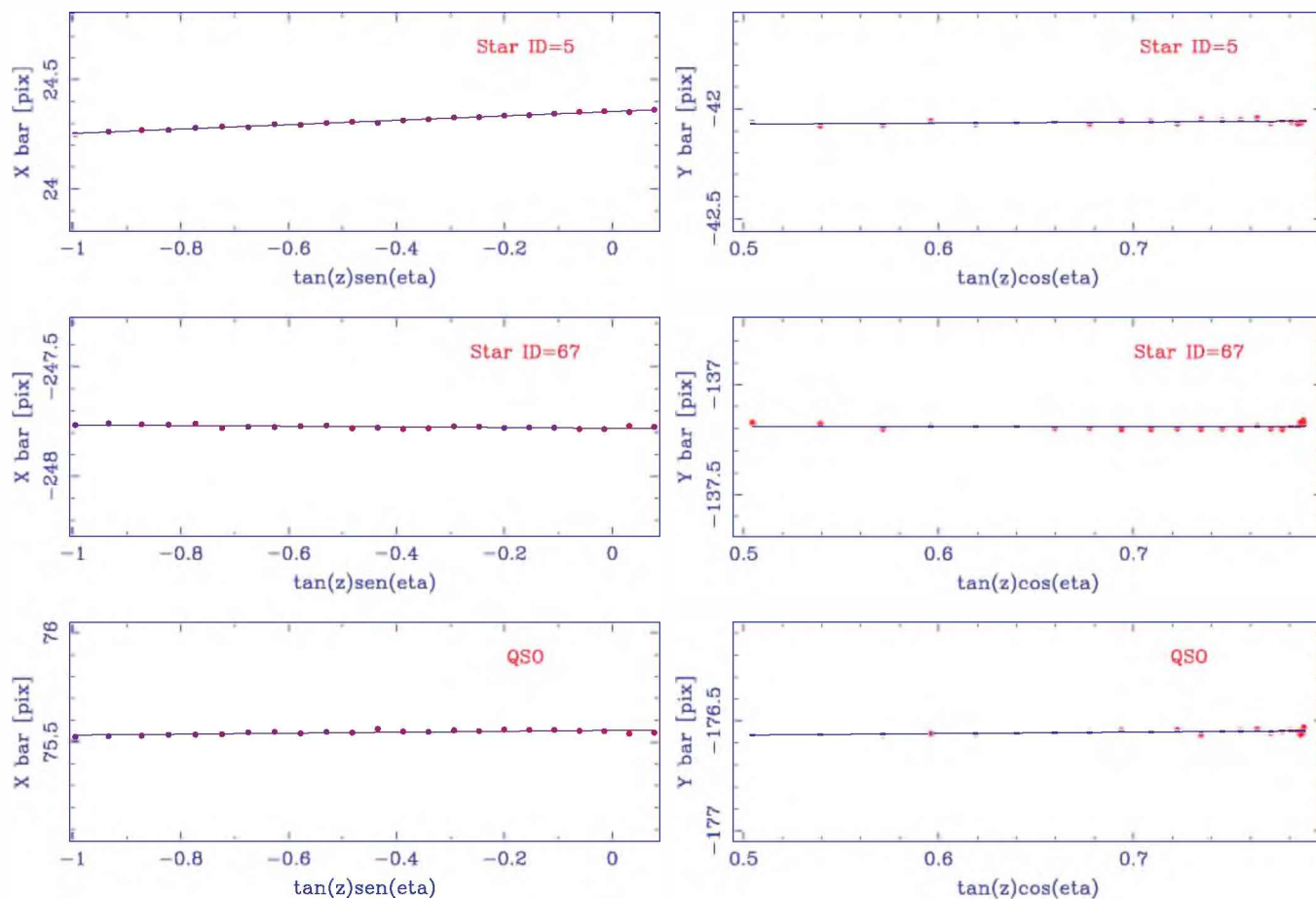
Figure 3. Example DCR series plot for two randomly selected reference stars, and the background QSO, in field QJ05570−6713 of the LMC. It is based on 23 off-meridian consecutive frames.

(A color version of this figure is available in the online journal.)

to evaluate dark current in our observing conditions, but it turned out to be negligible, so no correction for this effect was applied.

3. THE ASTROMETRY

3.1. The QSO Method

The method outlined here is the same used by ALP00, PAM02, and PCM06, where it is briefly described. Because the exact procedure was never fully explained in those earlier works, and because the analysis software was extensively revised and modified, in this paper we present a more detailed account of this method.

The QSO method is, in principle, quite simple. The position at different epochs of QSOs present in the background of the MCs is measured with respect to bona fide MC stars. Because QSOs can be considered fiducial points, any motion detected for them will be a reflection of the motion of the local field of MC stars.

3.2. Pixel Coordinates

The coordinates of the background QSOs and field stars on each CCD frame were determined using the various routines within the DAOPHOT package (Stetson 1987).

All frames available for each QSO field were first examined to identify, on the basis of image quality, the best of them (the "Master" frame) and also the best set of consecutive frames.

This latter set is used to establish a reference system with respect to which the motion of the QSO is measured—the "Standard Frame of Reference" (SFR)—and the Master frame is used to make a preliminary selection of the MC field stars that will define the SFR. All the above frames turned out to have stellar images with an average FWHM of ∼0″7.

By means of the DAOFIND and PHOT tasks, all objects down to an instrumental magnitude limit of ∼21 were automatically identified in the Master frame, which typically produced a list of ∼2000 objects. Their image profiles were examined on an individual basis to discard problematic objects (e.g., too close to a bad CCD column or to the edges, multiple objects not detected by DAOFIND, galaxies), and pairs of objects closer than ∼20 pixels (5″), peak-to-peak. This latter condition results from the fact that in all calculations the radius of the PSF model was chosen as 10 pixels. Pairs of objects marginally satisfying the above condition were also examined in the lesser quality frames (this because the PSFs of stars well separated on the Master frame can blend on poorer seeing images). With this procedure roughly 300 (depending on the stellar density of each field) isolated, well exposed (S/N better than ∼150), and homogeneously distributed stars were selected in each field. This set of stars defines the *initial* local reference system common to all frames of a given QSO field. It should be noted that this procedure to select an initial set of reference stars is purely morphological, and that no other criteria were applied a priori to exclude galactic foreground objects.
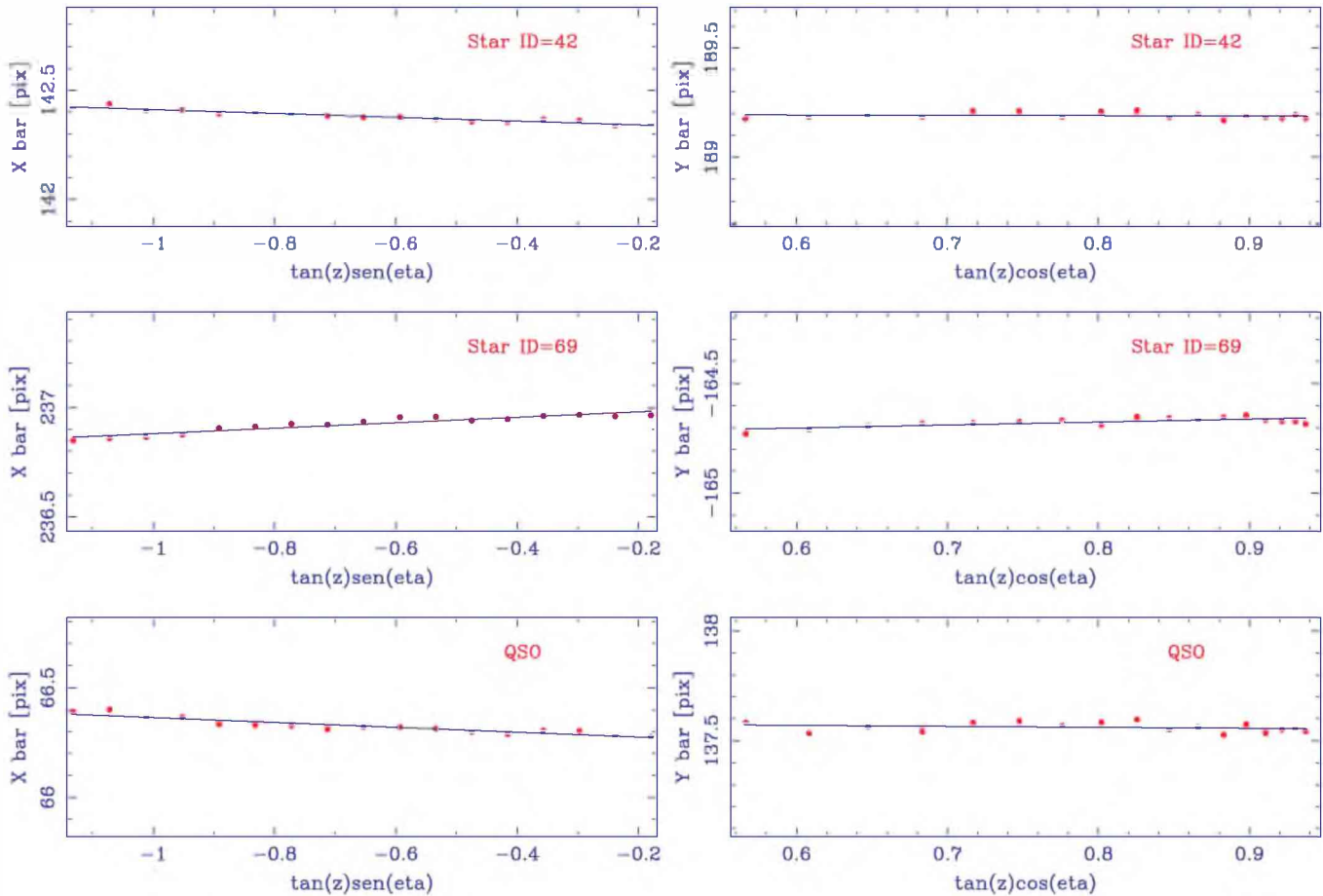
Figure 4. Example DCR series plot for two randomly selected reference stars, and the background QSO, in field QJ0036−7227 of the SMC. It is based on 17 off-meridian consecutive frames.

(A color version of this figure is available in the online journal.)

Additional cleansing, to ensure that each local reference system is composed only of MC stars, is done at a later stage (see Section 3.6).

A subset of typically 180 of the stars defining the initial local reference system in each QSO field was selected to determine a Master PSF for each frame available for that field. For this purpose we used the task PSF with *function = auto* and varorder = 2, thus allowing the PSF to vary with position on the CCD chip. A variety of experiments carried out to test the available centering algorithms and their centering parameters, confirmed that for our purposes the fitting radius is the most relevant parameter in the PSF fitting process. Given the conditions in which the reference stars were chosen, the adopted fitting radius for any frame was always slightly larger than the average FWHM of its stellar images. Finally, and by means of the task PEAK, the Master PSFs were used to calculate the (X, Y) centroids of the QSO and reference stars.

Due to slight offsets and small rotations between different frames (especially between frames of different epochs), to ensure that all objects of interest identified in any given frame of a certain QSO field were the same ones selected in the corresponding Master frame, a simple X–Y matching program was applied, and the cross-identification was verified on the image display. It should be noted that the identification numbers given in our tables and figures are ID numbers from the PEAK task outputs. We kept these IDs because it helped trace possible problems.

3.3. Barycentric Coordinates

Because of their greater stability, which allows for a much better positional precision at this stage of our procedure (i.e., before final registration), all calculations starting at this point were carried out in barycentric coordinates. These coordinates are defined as $X_i - \overline{X}$, $Y_i - \overline{Y}$, where $(\overline{X}, \overline{Y})$ (the "barycenter") is the average of the (X, Y) coordinates of the reference stars. This procedure reduces the negative impact of small offsets between frames, poor guiding, etc. Except for slight optical distortions, centering uncertainties, and proper motion effects; and as long as all reference stars are found in all frames of a given QSO field, these coordinates should be the same for all of them.

3.4. Differential Color Refraction Correction

By making all astrometric observations in the R bandpass, we effectively minimized refraction effects, but, for very precise relative astrometry, DCR requires a special treatment. Because atmospheric refraction is wavelength dependent, stars of different spectral energy distribution (SED) suffer different amounts of refraction. In our case, given that the SED of the background QSOs is quite different from that of a typical MC field star, this effect is particularly important, and could induce a systematic shift of the QSO's coordinates with respect to the reference stars. The CMDs of the stars used to define the *final* local reference system in the two QSO fields reported in this paper (Figures 16 and 17 below) clearly shows that we are measuring a rather
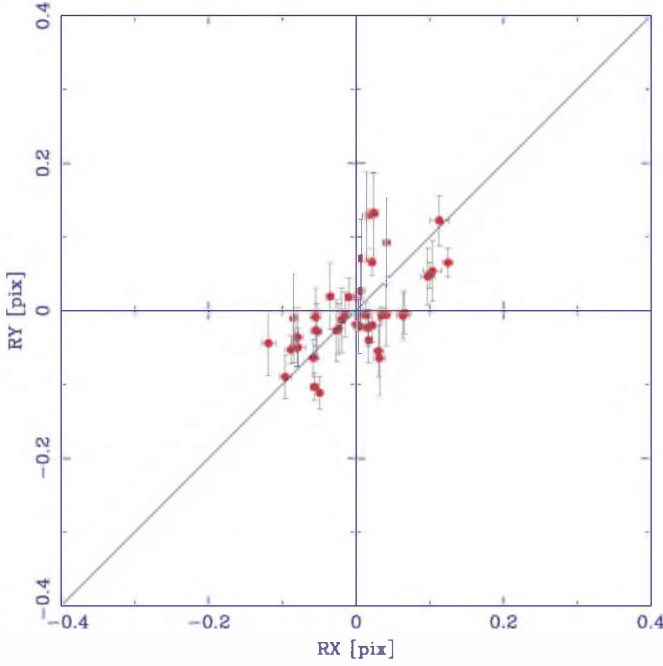
Figure 5. R_X vs. R_Y plot for the final reference stars, and the background QSO, in field QJ05570−6713; which shows the *nearly* one-to-one relationship between R_X and R_Y. The background QSO is depicted with a triangle.

(A color version of this figure is available in the online journal.)

Figure 6. Same as Figure 5, for field QJ0036−7227.

(A color version of this figure is available in the online journal.)

"bluish" object (the QSO) relative to a system composed mainly of MC red giants.

In Section 2 we mentioned that, to model the effect of DCR on the measured positions, DCR series were obtained. One series was secured per QSO field, this because the DCR correction to be applied is different for each of them. As explained in what follows, these observations allowed us to determine the shift due to DCR of the barycentric coordinates of the QSOs and the MC field reference stars as a function of hour angle.

If the unprimed quantities are the true values (not affected by refraction), and the prime quantities are affected by refraction, it can be shown that (see, e.g., Smart 1977)

$$\alpha - \alpha' = -R_\alpha \times \sec\delta' \tan z' \sin\eta', \qquad (1)$$

$$\delta - \delta' = -R_\delta \times \tan z' \cos\eta', \qquad (2)$$

where z' is the observed zenithal distance, and where R is the refraction constant, which depends on the wavelength of the incident light. In principle (see below), $R = R_\alpha = R_\delta$. The angle η' is given by
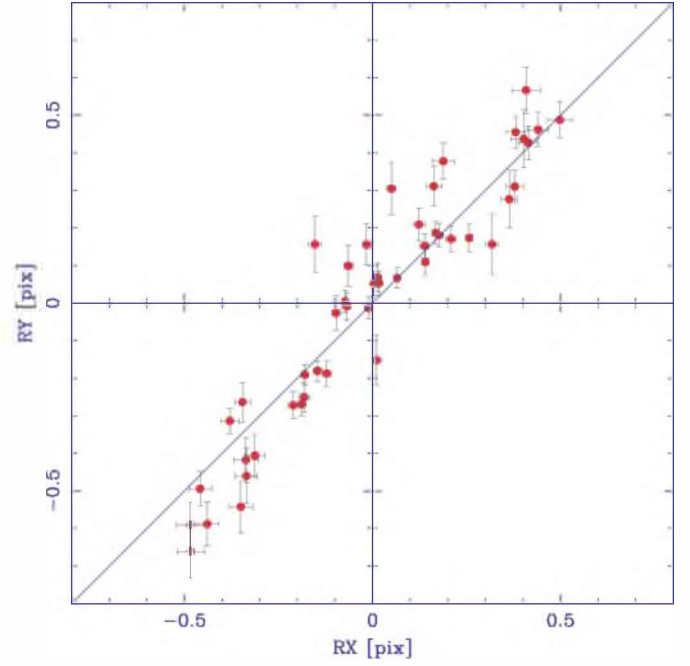
$$\sin\eta' = \frac{\cos\Phi\sin H'}{\sin z'}, \qquad (3)$$

$$\cos\eta' = \frac{\sin\Phi - \cos z'\sin\delta'}{\sin z'\cos\delta'}, \qquad (4)$$

Φ being the latitude of the observer, and H' the observed hour angle.

Given that our X and Y axes are oriented with R.A. and decl., respectively (see Section 3.8), these equations can also be written in the form

$$X - X' = -R_X \times \tan z'\sin\eta', \qquad (5)$$

$$Y - Y' = -R_Y \times \tan z'\cos\eta', \qquad (6)$$

where (X', Y') are noncorrected barycentric coordinates, and (X, Y) are barycentric coordinates corrected for DCR (to be determined).

The quantities R_X and R_Y are determined *individually* for each reference star and the QSO, by plotting their barycentric coordinates as a function of $\tan z'\sin\eta$ and $\tan z'\cos\eta$, respectively (for which we use the refraction series). The resulting plots are straight lines whose slopes are R_X and R_Y, and whose intercepts are the barycentric coordinates corrected for DCR.

Note that for each QSO field we have only one DCR series, so we have assumed that for a given field the same coefficients R_X, R_Y are valid for the entire epoch span of our study. As argued by Monet et al. (1992), this is indeed a reasonable assumption in our case. In Figures 3 and 4, we show example DCR series plots for objects in fields QJ05570−6713 (LMC) and QJ0036−7227 (SMC). They are based on 23 and 17 off-meridian consecutive frames, respectively. The corresponding QSOs and two randomly selected reference stars are shown in each case.

As mentioned before, in principle we should have $R_X = R_Y$, but in practice, due to errors, this is not exactly the case. As seen in Figures 3 and 4, the range in $\tan z'\sin\eta$ is larger than that in $\tan z'\cos\eta$ which allows for a more robust fit to determine R_X. In Figures 5 and 6, we present a plot of R_X versus R_Y for the objects of interest in fields QJ05570−6713 and QJ0036−7227, which shows that there is only a *nearly* one-to-one relationship between them. Please note the difference in the range of R_X and R_Y when comparing Figures 5 and 6. Based on these considerations, we have treated the two equations above as *independent*, and have calculated separate R_X and R_Y values for each reference star and the QSO.

In Figures 7 and 8, we present plots for the objects of interest in fields QJ05570−6713 and QJ0036−7227 showing the dependence of R_X and R_Y on the color of the objects.
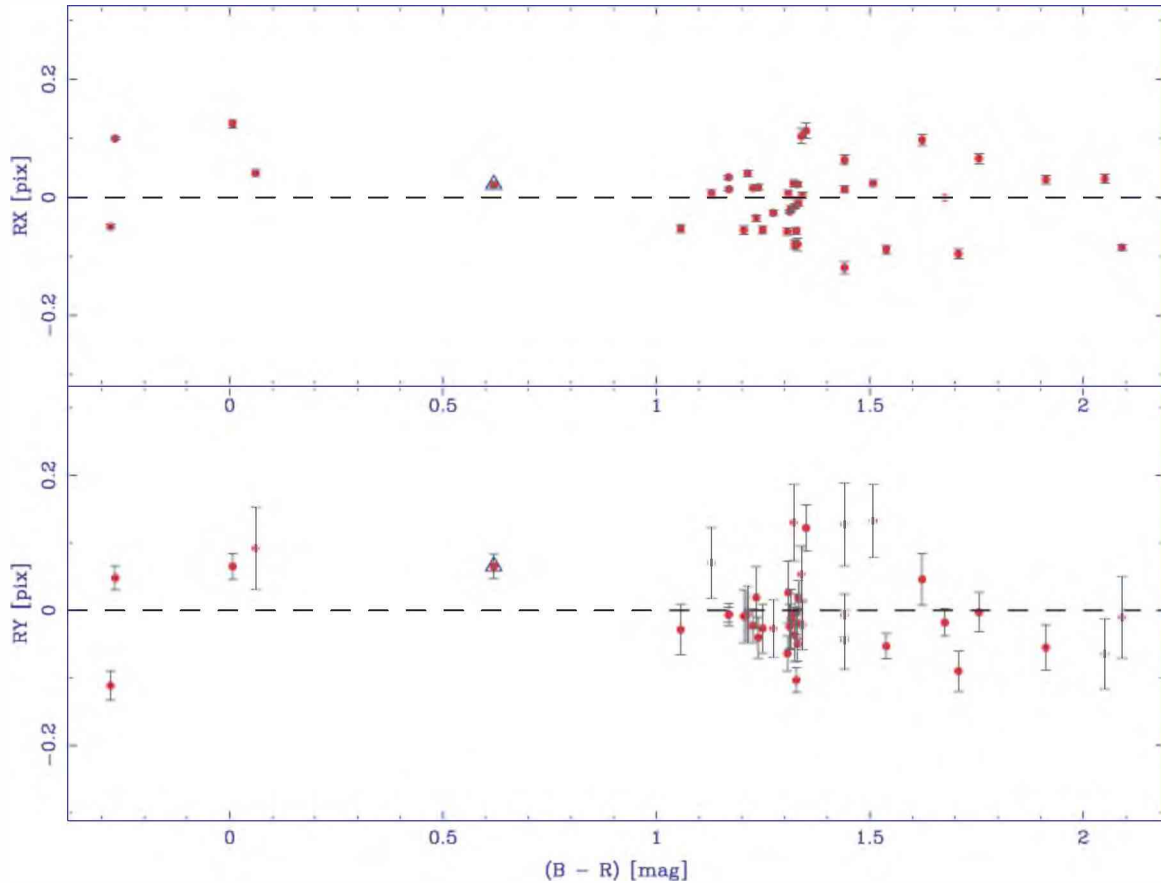
Figure 7. R_X vs. $(B - R)$ and R_Y vs. $(B - R)$ plots for the final reference stars, and the background QSO, in field QJ05570−6713, showing the dependence of R_X and R_Y on the color of the objects. Error bars where computed as the formal error of the slope in the straight-line fit to the DCR series plot of each object. The background QSO is depicted with a triangle.

(A color version of this figure is available in the online journal.)

They help illustrate the philosophy of the procedure, which is to correct the refraction constant of each object to bring it to the refraction constant corresponding to the mean color of the reference stars.

We note that after removing the effects of DCR from the data it is possible to include relatively large hour angle frames in the proper motion determination. Using the error in the final proper motion of the background QSO as an indicator, an iterative process was adopted to decide the maximum hour angle appropriate in each case. In this way we found that, in general, we could use all frames with $|HA| \leqslant 1.5$ hr.

Finally, having corrected the barycentric coordinates of all objects of interest for DCR, we redetermined the barycenter of the reference stars for all frames and therefore produced a new set of refraction-free barycentric coordinates.

3.5. Registration to the Standard Frame of Reference

The SFR is a reference system into which all images of a given QSO field (that is, the coordinates of all objects of interest in the field) are to be transformed. Measuring the position at different epochs of the background QSO with respect to the SFR leads in the end to the determination of the proper motion of the MC stars in the field.

The SFR is defined by the DCR-corrected barycentric co-ordinates of a set of bona fide MC field stars. In practice, the SFR is established by averaging the coordinates of these refer-ence stars in a set of consecutive, near meridian, good seeing

images (usually 3 or 4). The purpose of taking this average is to minimize the effect of centering errors in the construction of the SFR, which must be as representative as possible of the intrinsic geometrical distortions of the optical system. Because the average is done over barycentric coordinates, small guiding offsets in between these exposures are irrelevant.

The construction of the SFR is an iterative process; we start with the set of stars that define the *initial* local reference system selected for each QSO field as explained in Section 3.2, and progressively depurate it by eliminating objects that do not belong to the MCs, or are problematic in any way (see the following section).

The registration process itself is realized by means of a geometrical transformation. Given that all images are taken placing the QSO within a few pixels of a chosen position, it involves only minor shifts, rotations, scale changes, and higher order optical distortions. Registration was done using a standard χ^2 minimization algorithm over a multiple nonlinear regression polynomial (adapted from Bevington 1969). Numerous tests were carried out to select the proper terms and order of the polynomial to be used. These tests were made registering *intraepoch*, small hour angle ($|HA| \leqslant 1.0$ hr) consecutive R-band astrometric frames, because in these conditions there are no proper motions involved. They indicated that, in order to remove all trends in the residuals, and to minimize the rms of the transformation, a fourth-order polynomial in the coordinates was necessary. To avoid introducing noise with the inclusion of irrelevant terms for a given order, we explored the relevance
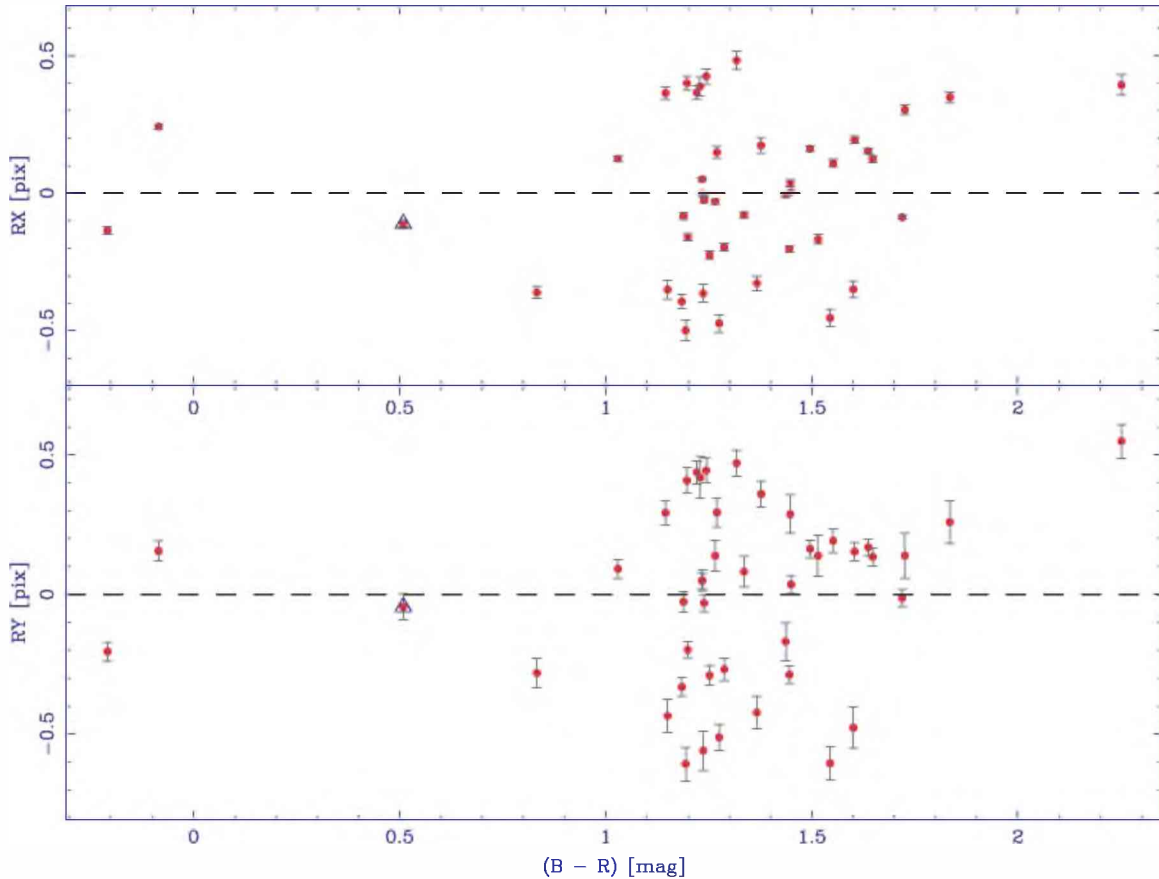
Figure 8. Same as Figure 7, for field QJ0036−7227.
(A color version of this figure is available in the online journal.)

of each of them. While some coefficients were small in certain cases, the same coefficients were large in others, so, given the large number of frames involved, we decided to include all terms up to the fourth order. It is important to note however, that *after* the local reference system is depurated from non-MC and problematic reference stars, there is no significant difference in the final result between a third- and a fourth-order registration. It is worth mentioning that Cudworth & Rees (1991) in their study of the optical distortions of the C100 telescope reported the need to use up to third-order terms. Their study, however, was based on photographic plates.

We shall call these coordinates resulting from the registration process "standard coordinates." Save for residual motions, caused by positional uncertainties, uncertainties in the DCR correction and in the registration process, the standard coordinates of true MC members will not change with time (assuming that our uncertainties are larger than any internal or streaming motion of the MC stars) in contrast to any object which does not conform to the SFR.

In Figures 9–11, we present example intraepoch residual plots (for a representative frame) for second-, third-, and fourth-order registrations, respectively. They were obtained plotting the differences $DX = (X_{std} − X_{sfr})$, $DY = (Y_{std} − Y_{sfr})$ between the standard coordinates (std) and the corresponding coordinates in the SFR (sfr) for the stars that define the initial local reference system, as a function of the coordinates in the SFR. These plots clearly show the need to include up to, at least, third-order terms in the registration process. The averages of the residuals for the example case are: $\sigma_X = 0.0075$ pixel, $\sigma_Y = 0.0109$ pixel

(order 2); $\sigma_X = 0.0070$ pixel, $\sigma_Y = 0.0087$ pixel (order 3); and $\sigma_X = 0.0067$ pixel, $\sigma_Y = 0.0069$ pixel (order 4). No residual trends as a function of the color or magnitude of the SFR stars were found (see the following section).

3.6. Cleansing of the Standard Frame of Reference

Plotting the standard coordinates of any object as a function of epoch allows us to determine its motion with respect to the SFR, through a linear regression. If we apply this procedure to the stars that define the initial local reference system for a given QSO field, we can identify objects with large motions, which must be excluded from the SFR. Because the initial reference system is selected in a purely morphological way (see Section 3.2), some objects in it could be Galactic foreground stars (producing a true motion) and others could have hidden companions or other problems affecting the astrometry (which will produce a spurious motion). In an iterative process, high motion stars are removed, the SFR is redefined, new standard coordinates are calculated, and thus new motions are determined. We do not have a strict rule to decide when to stop this iterative process; in its final steps the exclusion of stars is decided on the basis of its effect on the final error in the determination of the QSO's motion. Very loosely, we can, however, say that iterations are stopped approximately when $|\mu_i − \mu_{i−1}| \leqslant 3\sigma$, where $\sigma = \sqrt{\sigma_{\mu_i}^2 + \sigma_{\mu_{i−1}}^2}$, μ being the QSO's motion, and σ the final error of this motion.

The cleansing process of the SFR is perhaps the most critical step in the whole procedure; up to the elimination of objects
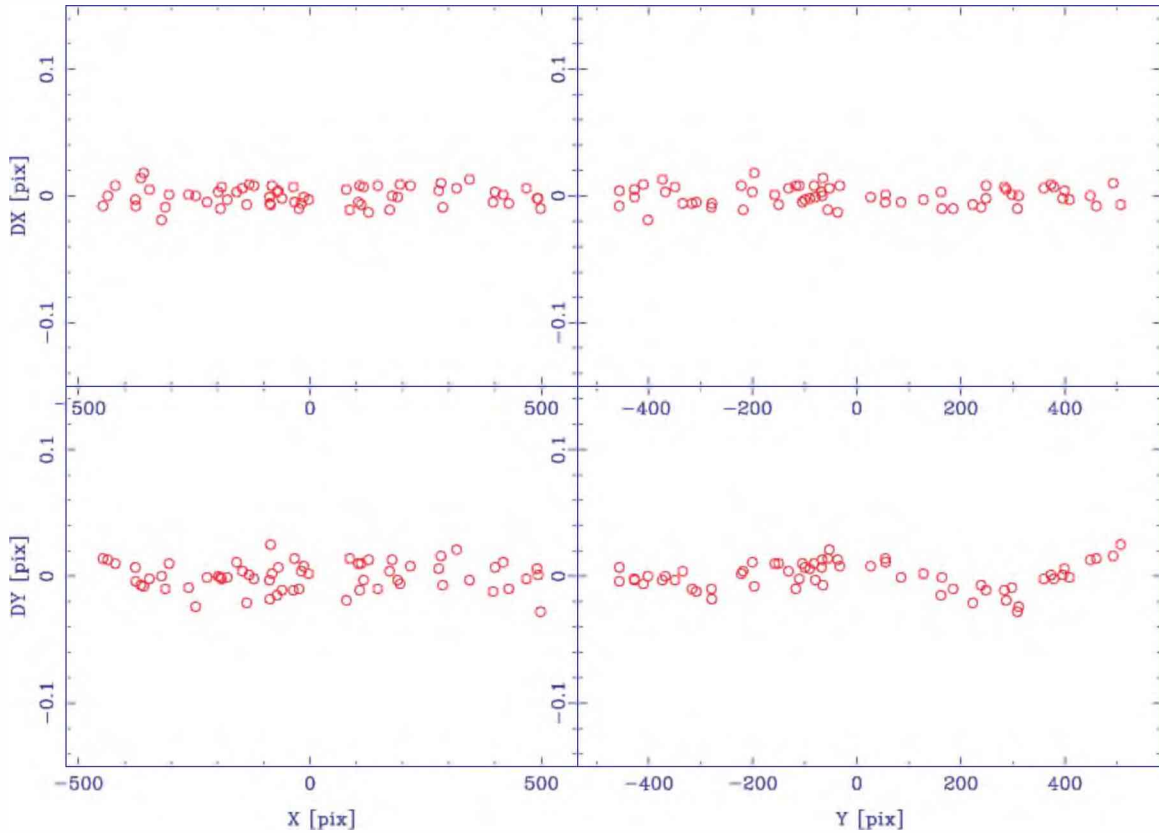
Figure 9. Example residual plot (for a randomly selected frame) for a second-order registration. It was obtained plotting the differences DX = $(X_{\text{std}} - X_{\text{sfr}})$, DY = $(Y_{\text{std}} - Y_{\text{sfr}})$ between the standard coordinates (std) and the corresponding coordinates in the SFR (sfr) for the stars that define the initial local reference system, as a function of the coordinates in the SFR. The average of the residuals is $\sigma_X = 0.0075$ pixel, $\sigma_Y = 0.0109$ pixel.

(A color version of this figure is available in the online journal.)

with motions larger than roughly 1 mas yr^{-1}, the final result can change substantially. In this context, it is mandatory that the SFR is composed by true MC members.

In the case of the LMC field QJ0557−6713, iterations were ended when the motion of the remaining reference stars was less than 0.5 mas yr^{-1} per coordinate, and in the case of the SMC field QJ0036−7227 when this motion was less than 0.7 mas yr^{-1} per coordinate. To put these values in perspective, we note that a Galactic halo field star with a velocity of 120 km s^{-1}, and at a distance of ∼25 kpc, will have a proper motion of 1.0 mas yr^{-1}; therefore, by restricting the SFR members to stars with motions less than this value, we are minimizing the chance of contamination by Galactic foreground objects.

It should be noted that in the final steps of the iteration process (i.e., after the removal of Galactic stars and problematic objects), we are dealing with motions whose magnitude is of the order of their errors. This is evident in Tables 3 and 4 (where rounded numbers are given). These residual motions (see below) are most probably due to the various sources of error affecting the standard coordinates. In this context, the difference in cut-off between our LMC and SMC QSO fields is a consequence of the larger errors involved in the latter case. Using the LMC cut-off (0.5 mas yr^{-1}) for the SMC leads to a sparse and inhomogeneous local reference system.

The number of reference stars in the final SFR was 41 objects in the case of field QJ0557−6713, and 44 objects in the case of field QJ0036−7227. Care was taken to end up with a distribution of stars as homogeneous as possible, centered on

the corresponding QSOs. As shown by Figures 12 and 13, this was indeed the case. In the case of field QJ0557−6713, to avoid contamination of our reference frame by stars from the compact LMC cluster NGC 2154 (subject of another investigation which resulted from the present program; see Baume et al. 2007), the selection of reference stars was restricted to the central part of the field. In the case of field QJ0036−7227, due to crowding, it was necessary to use the complete field of view in order to achieve an adequate number of reference stars.

If the final SFR stars are true MC members, they will share a common motion—save for their internal velocity dispersion—consistent with zero with respect to the barycenter of the SFR, different from that of the background QSO. This is certainly the case, as shown by Figures 14 and 15 which are residual (relative to the barycenter of the SFR) motion maps for the stars that define the SFR in fields QJ0557−6713 and QJ0036−7227, respectively. For the sake of clarity, we have included only the error bars of the QSOs. Error bars were computed as the formal error of the slope in the straight-line fit (see the following section), and thus include *all* the positional uncertainties mentioned before. It should be noted that the scatter seen on the SFR on these plots most probably stems entirely from random errors, and *does not* necessarily represent the velocity dispersion in these MC fields.

In Tables 3 and 4, we list the residual motions (relative to the barycenter of the field's SFR), together with *calibrated* photometric data, for the stars defining the local reference frames of fields QJ0557−6713 and QJ0036−7227, respectively.
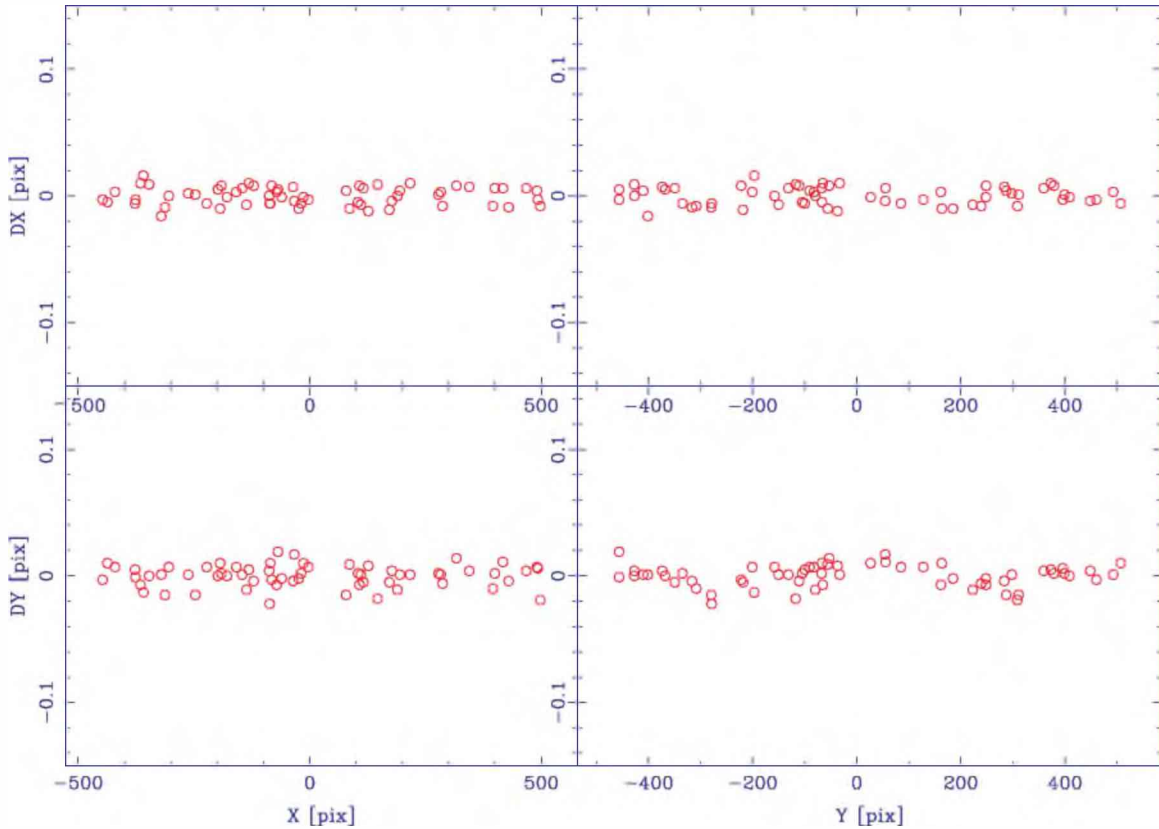
Figure 10. Example residual plot (for a randomly selected frame) for a third-order registration. It was obtained plotting the differences DX = $(X_{\rm std} - X_{\rm sfr})$, DY = $(Y_{\rm std} - Y_{\rm sfr})$ between the standard coordinates (std) and the corresponding coordinates in the SFR (sfr) for the stars that define the initial local reference system, as a function of the coordinates in the SFR. The average of the residuals is $\sigma_X = 0.0070$ pixel, $\sigma_Y = 0.0087$ pixel.

(A color version of this figure is available in the online journal.)

Weighted means and their respective standard deviations for the residual motions presented there are: 0.00 ± 0.18 mas yr^{-1} in R.A. and -0.00 ± 0.19 mas yr^{-1} in decl. (QJ0557−6713); 0.00 ± 0.26 mas yr^{-1} in R.A. and 0.00 ± 0.23 mas yr^{-1} in decl. (QJ0036−7227).

LMC photometry is from the related work by Baume et al. (2007) mentioned above. SMC photometry is from Noël et al. (2007), an investigation to study the star formation history of the SMC, which also resulted from the present program. The R versus $(B - R)$ CMDs presented in Figures 16 and 17 were constructed using the photometry cited. Examination of the QJ0557−6713 and QJ0036−7227 fields CMDs, and of those presented in Baume et al. (2007) and Noël et al. (2007), respectively, indicates that there is little or no contamination by Galactic foreground stars in the corresponding SFRs.

Before final cleansing of the SFR, we constructed CMDs to study possible dependencies of our proper motions on the color and brightness of the reference stars (caused in turn by population-dependent internal motions and/or unknown systematic astrometric effects). The number of blue objects among the initial reference stars turned out to be too small (LMC: 11 out of 88 stars; SMC: 6 out of 295 stars) for such tests to be meaningful. Nonetheless, tests were made to evaluate the effect of removing the (very few) blue reference stars seen in Figures 16 and 17 from the corresponding final SFR. In all cases, the exclusion of these stars increased the error of our final proper motions (albeit not changing the proper motion result substantially).

3.7. Proper Motions

As was the case with non-MC stars, the QSO does not conform to the SFR either, so its standard coordinates will also change with time. Because QSOs can be considered fiducial points, this motion with respect to the SFR is no more than the reflection of the motion of the local reference system of MC stars. This motion is also determined via a linear regression, and the *negative* slope of the straight line adjusted to the standard coordinates versus epoch diagram for the QSO will then give the proper motion of the corresponding MC field.

3.8. Results

In Tables 5 and 6, we give the mean barycentric positions of the background QSOs in fields QJ0557−6713 and QJ0036−7227 as a function of epoch, respectively, together with their standard deviations and the number of points used to calculate the mean for each epoch. In Figures 18 and 19, we present the corresponding barycentric position versus epoch diagrams. The values of R.A. and decl. in these figures are the individual positions of the QSOs on different frames relative to the barycenter (bc) of the SFR. The lines plotted are the best-fit lines resulting from a linear regression analysis on the data. The negative values of their slopes correspond to the actual proper motion of the barycenter of the reference stars.

For the LMC field QJ0557−6713, we have obtained ("as measured"; see Section 4)

$$\mu_{\alpha} \cos \delta = +1.95 \pm 0.13 \text{ mas yr}^{-1}.$$
$$\mu_{\delta} = +0.43 \pm 0.18 \text{ mas yr}^{-1}.$$
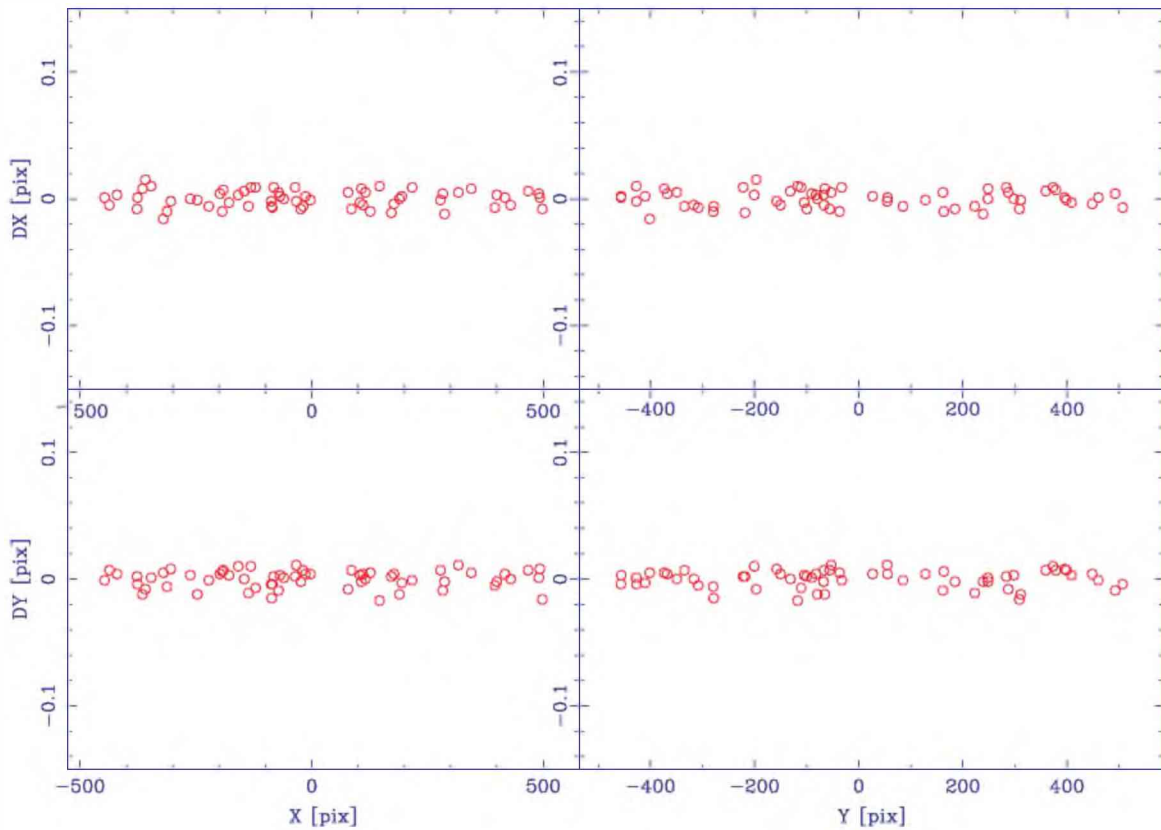
Figure 11. Example residual plot (for a randomly selected frame) for a fourth-order registration. It was obtained plotting the differences DX = $(X_{std} - X_{sfr})$, DY = $(Y_{std} - Y_{sfr})$ between the standard coordinates (std) and the corresponding coordinates in the SFR (sfr) for the stars that define the initial local reference system, as a function of the coordinates in the SFR. The average of the residuals is $\sigma_X = 0.0067$ pixel, $\sigma_Y = 0.0069$ pixel.

(A color version of this figure is available in the online journal.)

For the SMC field QJ0036−7227, we have obtained

$$\mu_\alpha \cos\delta = +0.95 \pm 0.29 \text{ mas yr}^{-1}.$$

$$\mu_\delta = -1.14 \pm 0.18 \text{ mas yr}^{-1}.$$

As mentioned in the Introduction, we also went through the full reduction procedure for the SMC field QJ0036−7225, but it was impossible to use it to derive a proper motion. The reason for this is the presence of a nearby star affecting the QSO's PSF, which posed an unsolvable reduction challenge. Since first inspection of the 10 SMC QSO fields, we were aware of this difficulty, but it was believed that a careful selection of the QSO's PSF parameters would be enough to deal with the situation. In spite of many tests, unfortunately this was not possible, and a set of data of comparable quality to that of field QJ0036−7227 was therefore lost (for astrometric purposes; not for our SFH program).

3.9. CCD Orientation

The proper motions derived above are in the approximate (R.A., decl.) directions given by the orientation of the corresponding SFR, which do not necessarily coincide with the Equatorial System for a given Equinox. To evaluate/correct for this possible effect, we have to find the orientation of the SFRs with respect to the International Celestial Reference frame (ICRF; Arias et al. 1995). This is done by comparison with the Guide Star Catalog, version 2.2 (GSC2.2, 2001).[7]

The registration into the coordinate system of the GSC2.2 uses the WCSTools 3.6.5 and 3.7.2 set of routines[8] developed by Doug Mink at CfA. Because this package works on images, it was necessary to select an image from each set defining the SFRs to carry out the procedure. Both in the case of QJ0557−6713 and QJ0036−7227, the Master frames were included in the SFRs, which made the selection straightforward. Our Master frames were found to have a negligible rotation with respect to the ICRF, namely, 0.73 ± 0.2 (QJ0557−6713) and 0.44 ± 0.2 (QJ0036−7227).

As a natural outcome of the procedure outlined above, a mean plate scale was obtained for the Master frames. From a set of 147 GSC stars identified in field QJ0557−6713 Master's frame, the plate scale turned out to be 0.2614 ± 0.0029 arcsec pixel^{-1}, and from a set of 56 GSC stars identified in field QJ0036−7227, it turned out to be 0.2559 ± 0.0028 arcsec pixel^{-1}. These values differ only ∼1% from the nominal plate scale (0.259 arcsec pixel^{-1}) so we used this latter throughout our study.

4. CENTER OF MASS PROPER MOTIONS

The proper motion results presented in Section 3.7 are "as measured" (field) values. If we want to derive the motion of the center of mass (CM) of the LMC or SMC, we have to remove (possible) perspective and rotation effects from our measured proper motions. The former is a purely geometric projection effect due to the angular separation in the sky between our

---

[7] Space Telescope Science Institute, 2001, The Guide Star Catalog, ver. 2.2.01.

[8] WCSTools is available at http://tdc-www.harvard.edu/software/wcstools/

Table 3
Local Reference Frame for the LMC Q0557−6713 Field

Star ID	$\mu_\alpha \cos\delta$ (mas yr^{-1})	σ (mas yr^{-1})	μ_δ (mas yr^{-1})	σ (mas yr^{-1})	R (mag)	B−R (mag)
5	−0.2	0.1	0.0	0.1	16.35	−0.27
6	0.2	0.1	−0.3	0.1	16.38	2.09
9	−0.1	0.1	−0.0	0.1	16.60	1.91
11	−0.1	0.1	−0.1	0.1	16.71	2.05
14	−0.0	0.1	0.1	0.1	16.94	1.17
17	0.2	0.1	−0.3	0.1	17.21	1.76
19	0.1	0.0	−0.1	0.0	17.36	1.44
21	−0.2	0.1	0.2	0.1	17.46	1.71
22	−0.1	0.1	0.1	0.1	17.48	1.06
23	0.3	0.1	−0.3	0.2	19.20	−0.28
25	0.1	0.1	0.3	0.1	17.74	1.68
26	−0.1	0.1	0.1	0.1	17.87	1.17
28	0.0	0.1	0.3	0.1	17.88	1.54
29	−0.0	0.1	0.1	0.1	17.92	1.51
30	0.3	0.1	0.2	0.1	17.97	1.21
33	0.0	0.1	−0.0	0.1	18.01	1.32
34	0.0	0.1	0.2	0.1	18.02	1.62
37	−0.1	0.1	0.1	0.1	18.18	1.25
38	−0.2	0.1	−0.3	0.1	18.19	1.31
39	0.1	0.1	0.1	0.1	18.24	1.31
42	−0.3	0.1	−0.1	0.1	18.31	1.23
44	−0.1	0.1	−0.4	0.1	18.44	1.32
47	−0.3	0.1	−0.0	0.1	18.52	1.35
49	0.3	0.1	−0.0	0.1	18.47	1.44
50	0.2	0.1	0.0	0.1	18.44	1.34
51	0.0	0.1	−0.2	0.1	18.47	1.33
53	−0.0	0.1	0.0	0.1	18.50	1.32
54	−0.2	0.1	−0.2	0.1	18.53	1.33
55	−0.1	0.1	0.1	0.1	18.58	1.21
56	0.2	0.1	0.1	0.1	18.60	1.33
57	0.4	0.1	0.2	0.1	18.55	1.31
59	−0.1	0.1	0.5	0.1	18.60	0.06
60	0.3	0.1	0.1	0.1	18.61	1.44
62	−0.1	0.1	−0.1	0.1	18.61	1.23
63	0.0	0.1	0.1	0.1	18.65	1.34
66	−0.2	0.1	0.1	0.1	18.65	1.33
67	0.2	0.1	−0.3	0.1	18.70	1.33
69	−0.4	0.1	−0.1	0.1	18.72	1.13
72	0.3	0.1	0.1	0.1	18.82	1.24
74	−0.1	0.1	0.0	0.1	18.82	0.01
77	−0.1	0.1	−0.2	0.1	18.93	1.27

Table 4
Local Reference Frame for the SMC Q0036−7227 Field

Star ID	$\mu_\alpha \cos\delta$ (mas yr^{-1})	σ (mas yr^{-1})	μ_δ (mas yr^{-1})	σ (mas yr^{-1})	R (mag)	B−R (mag)
12	0.4	0.1	−0.1	0.1	16.84	1.83
16	−0.3	0.1	0.1	0.1	16.89	2.25
42	−0.4	0.2	−0.7	0.2	17.06	1.72
47	−0.2	0.1	0.0	0.1	17.60	1.73
53	−0.2	0.2	0.2	0.1	17.71	−0.09
69	0.4	0.2	0.3	0.2	17.53	1.65
70	0.4	0.1	−0.1	0.2	17.99	1.60
75	−0.1	0.2	−0.1	0.1	17.58	1.55
76	−0.3	0.1	−0.4	0.1	17.62	1.64
102	0.0	0.1	−0.0	0.1	18.44	1.44
105	0.2	0.2	−0.1	0.2	18.04	1.54
106	0.3	0.1	0.2	0.3	18.08	−0.21
107	0.0	0.1	0.3	0.2	18.05	1.60
127	0.1	0.2	0.2	0.2	18.73	1.24
147	−0.2	0.2	0.2	0.2	18.84	1.14
154	0.3	0.2	−0.0	0.2	18.86	1.22
158	0.0	0.1	−0.0	0.1	18.44	1.44
159	−0.5	0.3	−0.0	0.2	18.97	1.20
160	−0.2	0.4	0.0	0.1	18.51	1.45
171	−0.1	0.1	−0.1	0.1	18.58	1.50
172	0.2	0.1	−0.1	0.2	19.06	1.23
173	−0.0	0.0	0.0	0.0	18.60	1.52
174	0.0	0.2	−0.1	0.1	18.55	1.03
178	0.4	0.2	−0.1	0.2	18.60	1.23
184	0.0	0.1	0.3	0.2	18.64	1.29
187	0.1	0.2	0.2	0.1	18.60	1.45
192	−0.1	0.2	0.1	0.2	18.64	1.24
197	−0.5	0.1	0.2	0.1	18.68	1.25
209	0.1	0.3	−0.1	0.2	18.80	1.19
210	0.5	0.3	−0.1	0.1	18.81	1.38
213	0.3	0.2	−0.2	0.1	18.73	1.37
218	−0.1	0.2	−0.0	0.1	18.74	1.23
227	0.0	0.1	0.2	0.1	18.83	1.19
230	0.0	0.2	0.1	0.2	18.87	1.18
234	−0.3	0.1	0.4	0.1	18.87	1.27
235	0.2	0.1	0.1	0.2	18.85	1.45
249	−0.1	0.1	−0.3	0.1	18.88	1.28
250	−0.4	0.2	−0.5	0.1	18.98	1.15
257	−0.5	0.2	0.4	0.2	18.91	1.27
260	0.3	0.1	−0.2	0.1	18.88	1.34
276	−0.2	0.2	0.3	0.2	19.06	1.24
277	0.1	0.2	−0.2	0.2	19.09	1.20
280	0.0	0.2	0.0	0.2	19.06	0.83
286	0.2	0.3	−0.1	0.2	19.71	1.32

fields and the corresponding CM, and the latter is due to internal systemic motions.

To accomplish this we have applied the method presented by Jones et al. (1994, hereafter JKL94). In this method, it is assumed that all the field stars are at the same distance, in the plane of the LMC disk, and that there is no contamination from a kinematical halo. Required input parameters are the equatorial coordinates of the field of interest (defined by the coordinates of the background QSO) and of the center of the galaxy, the heliocentric distance of the center of the galaxy, the inclination of the galaxy's disk and position angle (P.A.) of the line of the nodes, and the rotational velocity and radial velocity at the position of the field of interest.

More recently, van der Marel et al. (2002, hereafter vDM02) have proposed a more sophisticated method which includes a rotation curve and modern values for critical parameters such as the P.A. of the line of the nodes and the inclination of the LMC's disk. To evaluate the difference in the final result between both methods, we applied the JKL94 procedure— but using the new parameters given in vDM02—to the field

proper motion obtained for field QJ0459−6427 by PAM02, and obtained results identical to those obtained by running vDM02's full procedure to PAM02's field proper motion (see vDM02, Appendix). We therefore decided to keep using the JKL94 method, because of its relative simplicity, and because it facilitated internal consistency checks and certain comparisons with previous results by our group, *but* we have used the new input parameters given in vDM02.

4.1. The LMC

The LMC rotates (see, e.g., vDM02), and the angular distance between field QJ0557−6713 and the CM of the LMC is ∼3.8, so both a perspective and a rotation correction must be applied to our derived proper motion.

We have adopted the following values for the required input parameters.
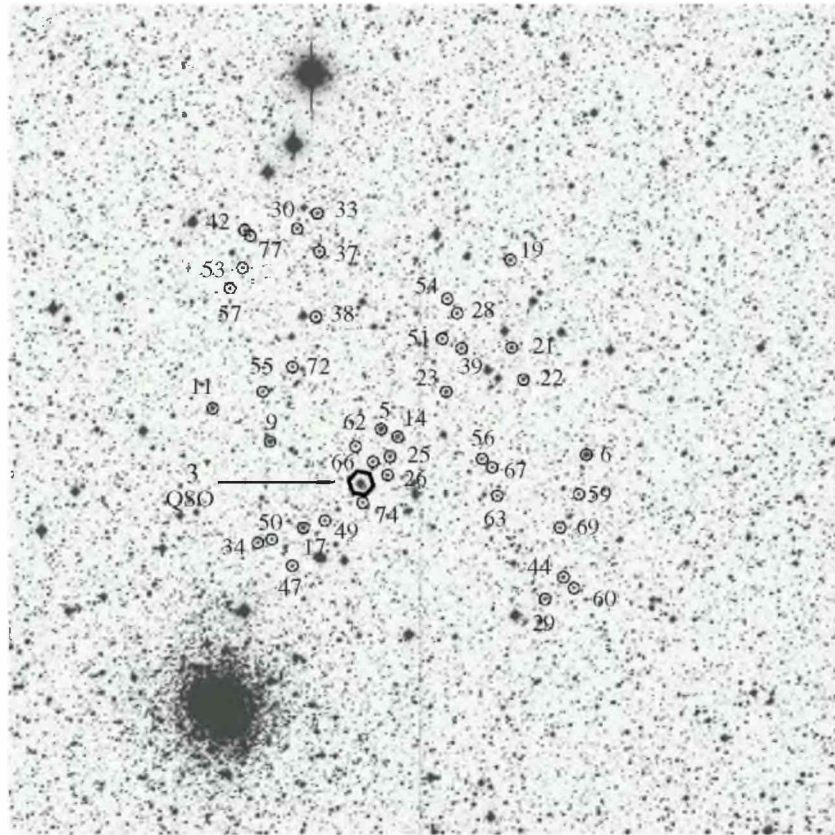
Figure 12. LMC field in the direction of the background quasar QJ0557−6713. The numbers identifying the QSO and reference stars are from our PEAK files. The compact LMC cluster in the field is NGC 2154, which was subject of another investigation (Baume et al. 2007). To avoid contamination of our reference frame by cluster stars, the selection of reference stars was restricted to the central part of the field. The size of the field is 8.85×8.85. North is at the top and east to the left.
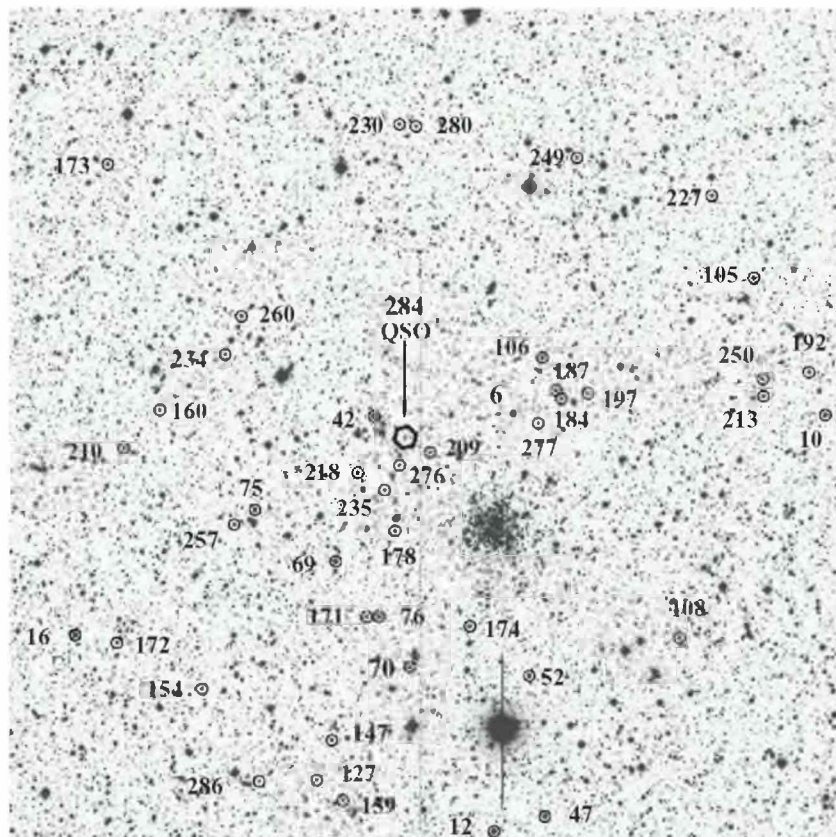
Figure 13. SMC field in the direction of the background quasar QJ0036−7227. The numbers identifying the QSO and reference stars are from our PEAK files. The sparse SMC cluster in the field is Kron 11 = Lindsay 20. Due to crowding (background is diminished in this finder), it was necessary to use the complete field of view in order to achieve an appropriate number of reference stars. The size of the field is 8.85×8.85. North is at the top and east to the left.
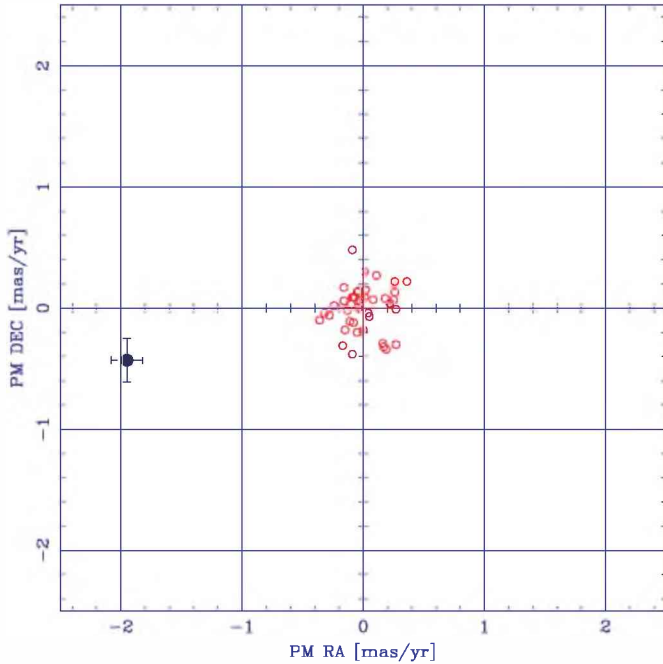
Figure 14. Residual motion map for the stars listed in Table 3, which define the reference frame in the LMC field of QJ0557−6713. The weighted mean and standard deviations for the residual motions presented in Table 3 are: 0.00 ± 0.18 mas yr^{-1} in R.A. and −0.00 ± 0.19 mas yr^{-1} in decl.

(A color version of this figure is available in the online journal.)

Field coordinates: (R.A., decl.) = (89°33, −67°22) J2000.0, from Blanco & Heathcote (1986).

LMC Center: (R.A., decl.) = (81°90, −69°87) J2000.0; kinematical center, from van der Marel & Cioni (2001).

Heliocentric distance of the LMC center: 50.1 kpc, corresponding to a distance modulus of $m−M = 18.5$, from Freedman et al. (2001).

Inclination of the disk: ($i = 34°7$), and P.A. of the descending node of the lines of nodes: (−50°1), both from vDM02. It should be noted that the values for the disk inclination and P.A. from vDM02 differ *considerably* from those used in JKL94, which has an important effect in the final value for the CM proper motion of the LMC.

Because we do not have a measured radial velocity for our LMC field, we have used the method proposed by JKL94 in which the radial velocity of a field must be such that the derived radial velocity for the CM of the LMC corresponds to standard values for this quantity in the literature (e.g., +262.1 km s^{-1}; vDM02). This procedure certainly introduces an uncertainty in the corrections, because it is known that bona fide LMC stars can have a large range in radial velocities, +170 ⩽ V_r ⩽ +380 km s^{-1} (Zhao et al. 2003; Carrera et al. 2008). To achieve the above, we adopted +287.0 km s^{-1} as the radial velocity for field QJ0557−6713.

Studies of the rotation of the LMC agree on a model rotation curve for the plane of the LMC, in which V_{rot} increases more or less linearly with radial distance in the plane up to a distance of ∼4 kpc, and is roughly constant at greater distances (see, e.g., vDM02; Olsen & Massey 2007; PI08). Depending on the kinematic tracer used, the maximum (constant) value of V_{rot} observed falls between ∼50 km s^{-1} and ∼120 km s^{-1}. Because our LMC field lies at a radius at which V_{rot} is maximum, the exact value adopted for the rotational velocity has an important effect on the rotation correction. To emphasize this we have calculated a CM proper motion of the LMC for the

two extreme values: 50 km s^{-1} (vDM02) and 120 km s^{-1} (PI08).

After applying the perspective/rotation corrections to our QJ0557−6713 field proper motion, we finally obtain

$$\mu_\alpha \cos\delta = +1.82 \pm 0.13 \, \text{mas yr}^{-1}$$
$$\mu_\delta = +0.39 \pm 0.15 \, \text{mas yr}^{-1} (V_{rot} = 50 \, \text{km s}^{-1})$$

and

$$\mu_\alpha \cos\delta = +1.61 \pm 0.13 \, \text{mas yr}^{-1}$$
$$\mu_\delta = +0.60 \pm 0.15 \, \text{mas yr}^{-1} (V_{rot} = 120 \, \text{km s}^{-1})$$

for the CM proper motion of the LMC.

4.2. The SMC

Contrary to what is observed in the LMC, there is no clear evidence of rotation in the case of the SMC (see, e.g., PI08), so a rotation correction to our field proper motion for field QJ0036−7227 is not needed. On the other hand, this field lies at an angular distance of ∼1°2 from the main body of the SMC, so a perspective correction is still required. To realize the latter via the JKL94 procedure, we have to assume that the SMC has a disklike central structure—an assumption which is supported by the results of Stanimirović et al. (2004)—and that field QJ0036−7227 lies in the principal plane of this disklike component.

We have adopted the following values for the required input parameters:

Field coordinates: (R.A., decl.) = (9°17, −72°46) J2000.0, from Tinney et al. (1997).

SMC center coordinates: (R.A., decl.) = (13°20, −72°50) J2000.0; kinematical center, from PI08.

Heliocentric distance of the SMC center: 61.7 kpc, corresponding to a distance modulus of $m−M = 18.95$, from Cioni et al. (2000).

Inclination of the disk: ($i = 40°$), from Stanimirović et al. (2004). P.A. of the descending node of the lines of nodes: (40°), also from Stanimirović et al. (2004).

For consistency with the LMC procedure, we also applied the JKL94 method explained in the previous section. Adopting +139.6 km s^{-1} as the radial velocity of field QJ0036−7227, yields the currently accepted radial velocity for the CM of the SMC (+146.0 ± 0.6 km s^{-1}; Harris & Zaritsky 2006). Interestingly, Carrera (2006) and Carrera et al. (2008) obtain a radial velocity at the position of our field of +145.0 km s^{-1}. It should be noted however that the stars targeted by Carrera in field QJ0036−7227 are not the same we used to define our reference system.

After applying the corrections, we finally obtain

$$\mu_\alpha \cos\delta = +1.03 \pm 0.29 \, \text{mas yr}^{-1},$$
$$\mu_\delta = -1.09 \pm 0.18 \, \text{mas yr}^{-1}$$

for the CM proper motion of the SMC.

4.3. Membership of the MCs to a Stream of Galaxies

Lynden-Bell & Lynden-Bell (1995), have proposed that the MCs, together with Draco and Ursa Minor (and possibly Carina and Sculptor), define a stream of galaxies (their stream 2) with similar orbits around our Galaxy. Their models predict
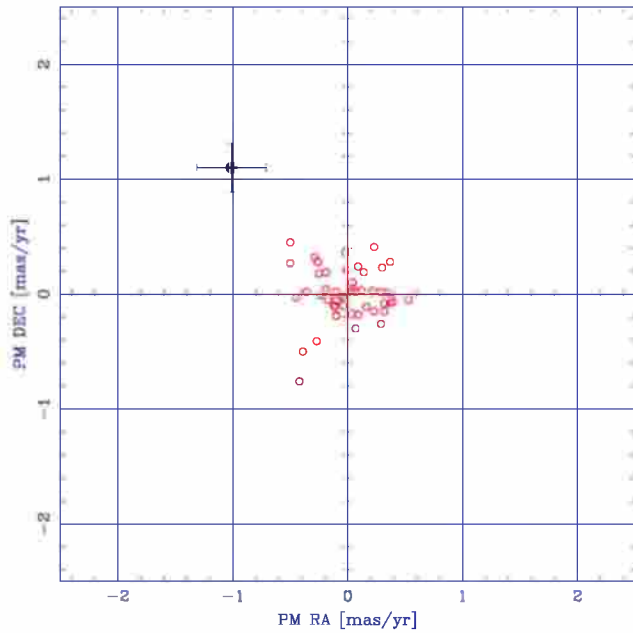
Figure 15. Residual motion map for the stars listed in Table 4, which define the reference frame in the SMC field of QJ0036−7227. The weighted mean and standard deviations for the residual motions presented in Table 4 are: 0.00 ± 0.26 mas yr^{-1} in R.A. and 0.00 ± 0.23 mas yr^{-1} in decl.

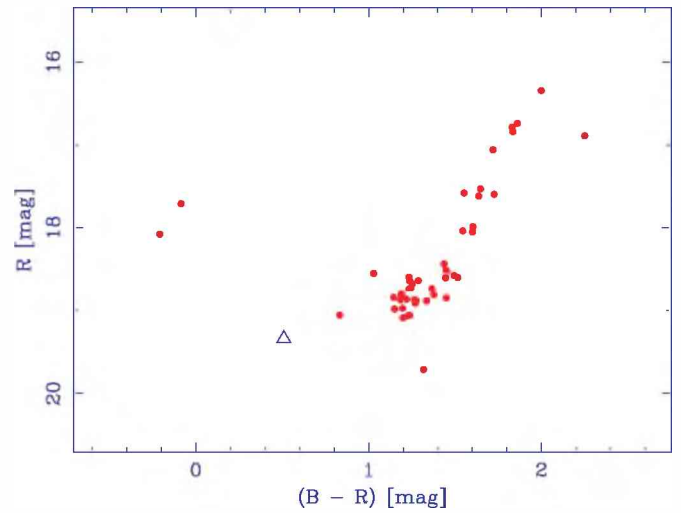(A color version of this figure is available in the online journal.)
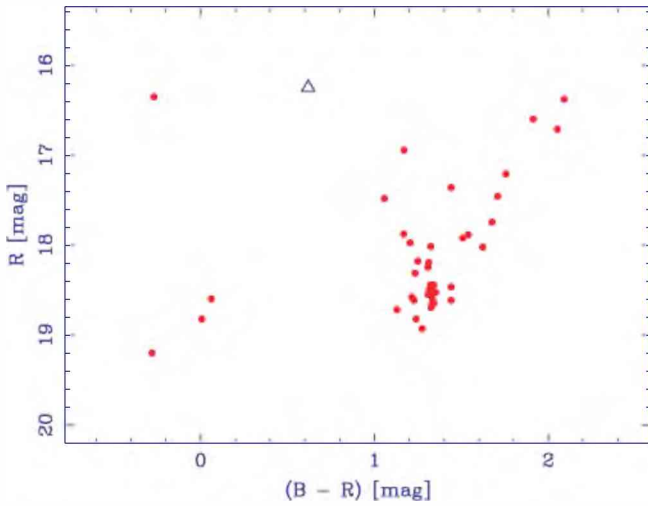
Figure 16. R vs. $(B - R)$ CMD of the stars used to define the reference frame in the field of QJ0557−6713. The background QSO is indicated by a triangle. This diagram was constructed using calibrated photometry obtained for the LMC field QJ0557−6713 by Baume et al.(2007), in the course of their study of the LMC cluster NGC 2154. Examination of the present diagram and of that given in the above reference indicates that there is little or no contamination by Galactic foreground stars.

(A color version of this figure is available in the online journal.)

heliocentric proper motions for each member of the stream, which can be compared to our heliocentric CM proper motions to evaluate the reality of this stream.

For the LMC they predict heliocentric proper motion components of $(\mu_\alpha \cos\delta, \mu_\delta) = (+1.5, 0)$ mas yr^{-1}, giving a total proper motion of $\mu = +1.50$ mas yr^{-1}, with a P.A. of $\theta = 90°$. Our LMC CM proper motion components: $(+1.82 \pm 0.13, +0.39 \pm 0.15, V_{rot} = 50$ km s^{-1}), or $(+1.61 \pm 0.13, +0.60 \pm 0.15, V_{rot} = 120$ km s^{-1}), imply a total proper motion of $\mu = +1.86 \pm 0.13$ mas yr^{-1}, with a P.A. of $\theta = 78 \pm 2°$, and $\mu = +1.72 \pm 0.13$ mas yr^{-1}, with a P.A. of $\theta = 70 \pm 3°$, respectively. Our μ and θ

Figure 17. R vs. $(B - R)$ CMD of the stars used to define the reference frame in the field of QJ0036−7227. The background QSO is indicated by a triangle. This diagram was constructed using calibrated photometry obtained for the SMC fields QJ0036−7225 and QJ0036−7227 by Noël et al. (2007), in the course of their study of the star formation history of the SMC. Examination of the present diagram and of that given in the above reference indicates that there is little or no contamination by galactic foreground stars.

(A color version of this figure is available in the online journal.)

Table 5
Mean Barycentric Positions of QJ0557−6713 (LMC)

Epoch	$\overline{\alpha}_{bc}$	σ	$\overline{\delta}_{bc}$	σ	N
	(arcsec)	(mas)	(arcsec)	(mas)	
2001.799	19.466	0.5	−45.792	0.8	12
2002.781	19.468	0.6	−45.797	0.4	19
2003.814	19.468	0.3	−45.797	0.5	19
2004.849	19.465	0.3	−45.795	1.2	10
2005.833	19.463	0.3	−45.800	0.5	33
2006.807	19.458	0.2	−45.795	0.5	31

Table 6
Mean Barycentric Positions of QJ0036−7227 (SMC)

Epoch	$\overline{\alpha}_{bc}$	σ	$\overline{\delta}_{bc}$	σ	N
	(arcsec)	(mas)	(arcsec)	(mas)	
2001.798	17.243	1.2	35.597	1.3	10
2002.782	17.240	3.0	35.597	0.9	6
2003.813	17.236	1.5	35.598	1.5	3
2005.832	17.239	1.6	35.600	1.1	7
2006.807	17.239	1.2	35.601	1.0	8
2007.775	17.235	1.0	35.604	1.1	8

values are 2.7σ and 6.3σ ($V_{rot} = 50$ km s^{-1}) or 1.7σ and 6.4σ ($V_{rot} = 120$ km s^{-1}) away from the predicted values. For the SMC their prediction is: $(\mu_\alpha \cos\delta, \mu_\delta) = (+0.7, -1.1)$ mas yr^{-1}, giving a total proper motion of $\mu = +1.28$ mas yr^{-1}, with a P.A. of $\theta = 149°$. Our SMC CM proper motion components: $+1.03 \pm 0.29, -1.09 \pm 0.18$ imply a total proper motion of $\mu = +1.49 \pm 0.23$ mas yr^{-1}, with a P.A. of $\theta = 137 \pm 15°$, values which are 0.9σ and 0.8σ away from the predictions, respectively.

These differences imply that the SMC could be a member of the above stream, while the LMC probably not. If we assume that the MCs are gravitationally bound, this result is not consistent, and questions the reality of the proposed stream. It is worth noting that Piatek et al. (2005) have also concluded that Ursa Minor is not a member of stream 2. In Section 6, we further discuss the gravitational binding of the MCs.
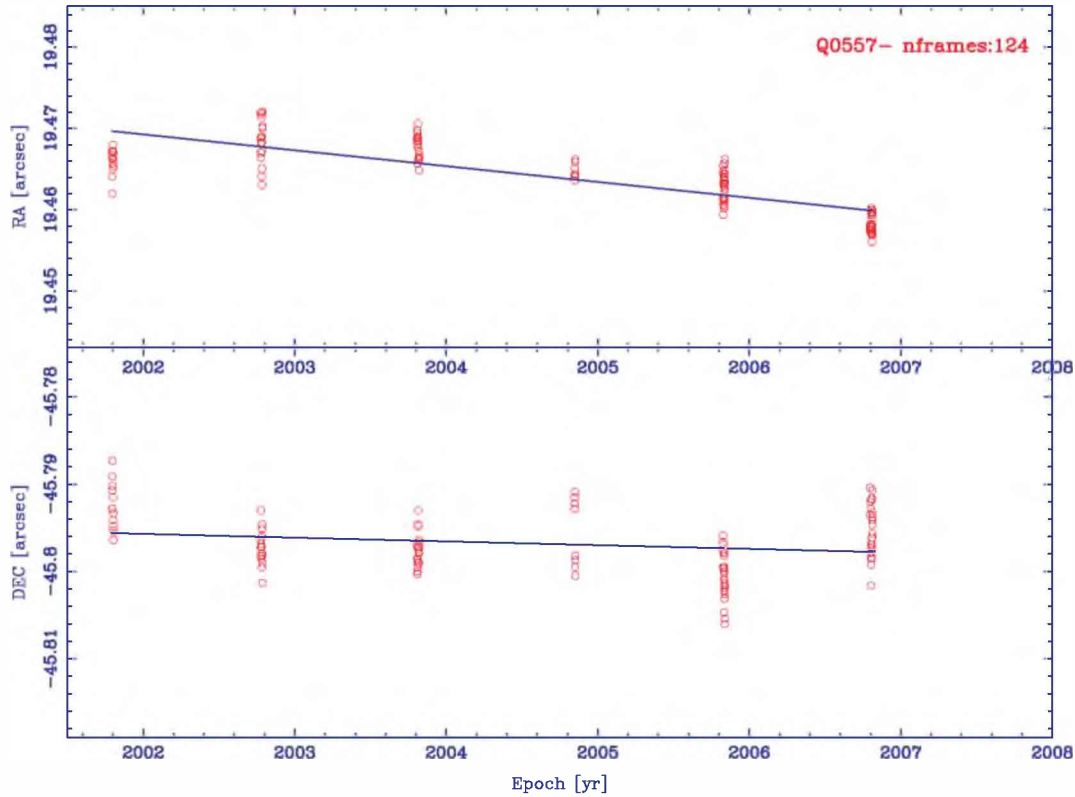
Figure 18. Barycentric position vs. Epoch diagram for QJ0557−6713. The values of R.A. and decl. are the individual positions of the QSOs on different frames relative to the barycenter (bc) of the SFR. The lines shown are the best-fit lines resulting from a linear regression analysis on the data. The *negative* values of their slopes correspond to the actual proper motion of the barycenter of the LMC reference stars: $\mu_\alpha \cos\delta = +1.95 \pm 0.13$ mas yr^{-1}. and $\mu_\delta = +0.43 \pm 0.18$ mas yr^{-1}.
(A color version of this figure is available in the online journal.)

Table 7
Proper Motion Determinations for the LMC

Source	$\mu_\alpha \cos(\delta)$	μ_δ	Proper Motion System
	(mas yr^{-1})	(mas yr^{-1})	
Kroupa et al. 1994 (F)	$+1.3 \pm 0.6$	$+1.1 \pm 0.7$	PPM
JKL 1994 (CM)	$+1.37 \pm 0.28$	-0.18 ± 0.27	Galaxies
Kroupa & Bastian 1997 (F)	$+1.94 \pm 0.29$	-0.14 ± 0.36	*Hipparcos*
ALP00 (CM)	$+1.7 \pm 0.2$	$+2.9 \pm 0.2$	QSO
Drake et al. 2001 (CM)	$+1.4 \pm 0.4$	$+0.38 \pm 0.25$	QSO
PAM02 (CM)	$+2.0 \pm 0.2$	$+0.4 \pm 0.2$	QSO
PCM06 (F)[a]	$+1.5 \pm 0.1$	$+1.4 \pm 0.1$	QSO
PCM06 (CM)[a]	$+1.8 \pm 0.1$	$+1.1 \pm 0.1$	QSO
K06b (F)[b]	$+1.97 \pm 0.09$	$+0.46 \pm 0.10$	QSO
K06b (CM)[c]	$+2.03 \pm 0.08$	$+0.44 \pm 0.05$	QSO
PI08 (CM)[d]	$+1.956 \pm 0.036$	$+0.435 \pm 0.036$	QSO
This work (Field)[e]	$+1.95 \pm 0.13$	$+0.43 \pm 0.18$	QSO
This work (CM)[e]	$+1.82 \pm 0.13$	$+0.39 \pm 0.15$	QSO
This work (CM)[f]	$+1.61 \pm 0.13$	$+0.60 \pm 0.15$	QSO

Notes. F: as measured field proper motion; CM: center of mass proper motion.
[a] Weighted mean of four QSO fields.
[b] Weighted mean of 13 QSO fields.
[c] Unweighted mean of 21 QSO fields.
[d] Weighted mean of 21 QSO fields.
[e] From one QSO field: Q0557−6713, $V_{\rm rot} = 50$ km s^{-1}.
[f] From one QSO field: Q0557−6713, $V_{\rm rot} = 120$ km s^{-1}.

5. COMPARISON WITH OTHER PROPER MOTION RESULTS

In Tables 7 and 8, we list all the available proper motion determinations for the LMC and SMC, respectively. F stands for field proper motions, while CM stands for center of mass proper

motions. Examination of these tables shows that our results are in reasonable agreement with most previous investigations of the proper motion of the MCs.

It is our opinion that a more detailed analysis based on the data presented in these tables is not appropriate. Proper motion values from different fields cannot be compared directly because they
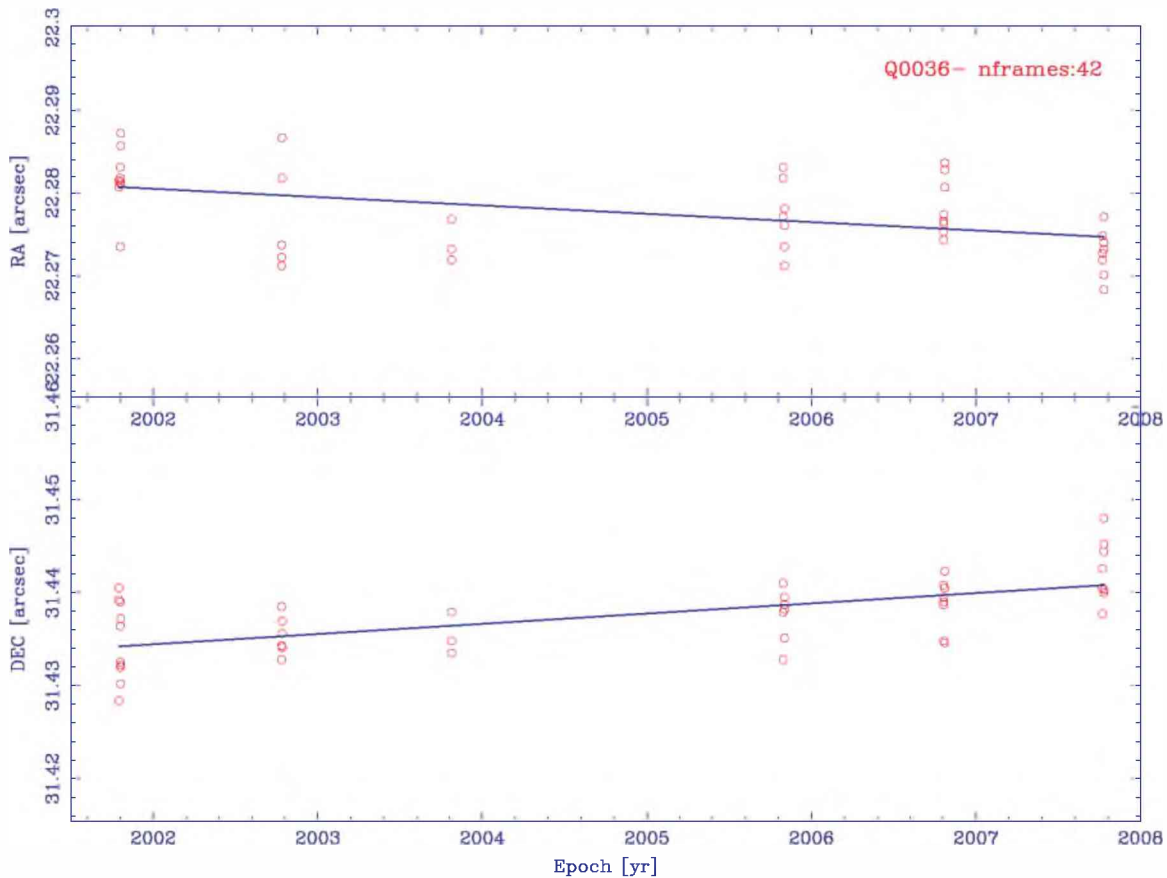
Figure 19. Barycentric position vs. Epoch diagram for QJ0036−7227. The values of R.A. and decl. are the individual positions of the QSOs on different frames relative to the barycenter (bc) of the SFR. The lines shown are the best-fit lines resulting from a linear regression analysis on the data. The *negative* values of their slopes correspond to the actual proper motion of the barycenter of the SMC reference stars: $\mu_\alpha \cos\delta = +0.95 \pm 0.29$ mas yr^{-1}, and $\mu_\delta = -1.14 \pm 0.18$ mas yr^{-1}.

(A color version of this figure is available in the online journal.)

Table 8
Proper Motion Determinations for the SMC

Source	$\mu_\alpha \cos(\delta)$	μ_δ	Proper Motion System
	(mas yr^{-1})	(mas yr^{-1})	
Kroupa et al. 1994 (F)	$+0.5 \pm 1.0$	-2.0 ± 1.4	PPM
Kroupa & Bastian 1997 (F)	$+1.23 \pm 0.84$	-1.21 ± 0.75	*Hipparcos*
K06a (F)[a]	$+1.16 \pm 0.18$	-1.17 ± 0.18	QSO
PI08 (CM)[b]	$+0.754 \pm 0.061$	-1.252 ± 0.058	QSO
This work (F)[c]	$+0.95 \pm 0.29$	-1.14 ± 0.18	QSO
This work (CM)[c]	$+1.03 \pm 0.29$	-1.09 ± 0.18	QSO

Notes. F: as measured field proper motion; CM: center of mass proper motion.
[a] Weighted mean of five QSO fields.
[b] Weighted mean of five QSO fields.
[c] From one QSO field: Q0036−7227.

are affected by different perspective and rotation effects. On the other hand, CM proper motions are obtained via an elaborated procedure in which various assumptions are made. To further complicate comparisons, all results may additionally be affected by *unidentified* systematic errors. A hint of the seriousness of this latter possibility is the fact that, for a given MC field, field proper motions from different groups show important discrepancies that in most cases cannot be explained.

In this context, it is important to note that the present results should be considered independent from those of ALP00, PAM02, and PCM06. Although the *basic* procedure was the

same, the instrumental setup was different (and therefore subject to different systematic effects), and the need to use higher orders in the registration polynomials constitutes an important difference.

SMC QSO field QJ0036−7227 was observed by K06a, but their result for this field was not included in their *final* calculation of the SMC proper motion; the reason for this being the great discrepancy between the proper motion they derived for this field and those derived for other four fields they targeted (see their Table 2 and Figure 7). More recently, PI08 have reprocessed K06's data, and, after removing the effect of trends with S/N,

have concluded that all five SMC targeted by *HST* contain useful information about the proper motion of the SMC. However, a look at Figure 5 of PI08 shows an important difference (particularly in R.A.) in the proper motion they measured for this field and those measured for the others. For this SMC field, the results of K06a: $\mu_\alpha \cos\delta = +0.303 \pm 0.073$ mas yr^{-1}, $\mu_\delta = -0.866 \pm 0.177$ mas yr^{-1}; and PI08: $\mu_\alpha \cos\delta = +0.438 \pm 0.115$ mas yr^{-1}, $\mu_\delta = -1.110 \pm 0.09$ mas yr^{-1}, are both discrepant with ours.

6. GALACTOCENTRIC SPATIAL VELOCITIES

We ultimately want to determine the space velocities of the LMC and SMC with respect to the center of our Galaxy, knowledge of which can be used to determine their orbits, and therefore the history of interactions between them, and with the MW. To accomplish this, we have to project our CM proper motions into the Galactic (μ_l, μ_b) system, and then calculate the velocity components in the Galactic (u, v, w) system. The second step requires knowledge of the radial velocities of the centers of the LMC and SMC, which we have adopted from the literature: $+262.1 \pm 3.4$ km s^{-1} (LMC; vDM02); $+146.0 \pm 0.6$ km s^{-1} (SMC; Harris & Zaritsky 2006).

The CM proper motions can be transformed to proper motions in the Galactic system by means of

$$\mu_l = \mu_\alpha \cos\delta \, \cos\eta + \mu_\delta \sin\eta,$$
$$\mu_b = -\mu_\alpha \cos\delta \, \sin\eta + \mu_\delta \cos\eta.$$

The "angle of the star," η, and the angular distance, χ, are given by

$$\sin\eta = \frac{\sin(\alpha - \alpha_p) \cos\delta_p}{\sin\chi}.$$
$$\cos\eta = \frac{\sin\delta_p - \cos\chi \, \sin\delta}{\sin\chi \cos\delta}.$$
$$\cos\chi = \sin\delta_p \, \sin\delta + \cos\delta_p \, \cos\delta \, \cos(\alpha - \alpha_p),$$

where $\alpha_p = 192°.86$, $\delta_p = +27°.13$, J2000, are the equatorial coordinates of the North Galactic Pole, and (α, δ) are the coordinates of the center of the LMC or SMC. Note that $\chi = 90 - b$, where b is the galactic latitude of the star.

We then compute velocities in the heliocentric (hc) Galactic system (u, v, w) through the equations

$$u_{\rm hc} = V_r \cos b \cos l - V_b \sin b \cos l - V_l \sin l$$
$$v_{\rm hc} = V_r \cos b \sin l - V_b \sin b \sin l + V_l \cos l$$
$$w_{\rm hc} = V_r \sin b + V_b \cos b,$$

where $V_l = 4.74 \, \mu_l \, R$ and $V_b = 4.74 \, \mu_b \, R$ are heliocentric velocities (km s^{-1}) in Galactic longitude and latitude, respectively, and R is the heliocentric distance (in kpc) of the CM of the LMC or SMC.

These heliocentric velocities include the solar peculiar motion and the motion of the LSR. One can obtain a velocity that corrects for the motion of the Sun around the Galactic center (Galactic Rest Frame, grf), which represents the motion of the MCs as seen from a reference point that is stationary with respect to the Galactic center, but located in the (instantaneous) solar position. These grf velocities, $\vec{V}_{\rm grf} = (u_{\rm grf}, v_{\rm grf}, w_{\rm grf})$, are related to the heliocentric velocities, $\vec{V}_{\rm hc}$, through

$$\vec{V}_{\rm grf} = \vec{V}_{\rm hc} + \vec{V}_\odot + \vec{V}_{\rm LSR}, \quad (7)$$

where $\vec{V}_\odot$ is the Solar peculiar motion with respect to the LSR, and $\vec{V}_{\rm LSR}$ is the speed of the LSR.

Throughout this paper, we have adopted $\vec{V}_\odot = (u_\odot, v_\odot, w_\odot) = (+10, +5.25, +7.17)$ km s^{-1}, and $\vec{V}_{\rm LSR} = (0, +220, 0)$ km s^{-1}, in the right-handed system where the (u, v, w) axes point toward the Galactic center, the sense of Galactic rotation, and the North Galactic Pole, respectively (Dehnen & Binney 1998).

To compute the CM velocities as seen from the Galactic center (galactocentric (gc) velocities), $\vec{V}_{\rm gc} = (\Pi, \Theta, Z)$, and not from the (instantaneous) position of the Sun as given by Equation (7), we have to correct for a perspective effect. The geometry of the situation shows that $(\Pi, \Theta, Z) = (-u_{\rm grf}, v_{\rm grf}, w_{\rm grf})$. The Π component is parallel to the radius vector from the Galactic center to the Sun, and points in the direction opposite to the galactic center; the Θ component is parallel to the Galactic plane and points in the direction of rotation of the Galactic disk and the Z component points in the direction of the North Galactic Pole.

The radial $V_{\rm gc,r}$ and tangential $V_{\rm gc,t}$ gc velocities in the (left-handed) system given by the unitary vectors $(\vec{e}_{\rm r}, \vec{e}_{\rm l}, \vec{e}_{\rm b})$ (for analogy to the corresponding unitary vectors as seen from the Sun), are given by

$$V_{\rm gc,r} = \Pi \cos b_{\rm gc} \cos l_{\rm gc} + \Theta \cos b_{\rm gc} \sin l_{\rm gc} + Z \sin b_{\rm gc}, \quad (8)$$

$$V_{\rm gc,b} = -\Pi \sin b_{\rm gc} \cos l_{\rm gc} - \Theta \sin b_{\rm gc} \sin l_{\rm gc} + Z \cos b_{\rm gc}, (9)$$

$$V_{\rm gc,l} = -\Pi \sin l_{\rm gc} + \Theta \cos l_{\rm gc}, \quad (10)$$

$$V_{\rm gc,t} = \sqrt{V_{\rm gc,l}^2 + V_{\rm gc,b}^2}. \quad (11)$$

The angles $(l_{\rm gc}, b_{\rm gc})$ are given by

$$\cos l_{\rm gc} = \frac{R_\odot - d \cos b \cos l}{R_{\rm pl}}.$$
$$\sin l_{\rm gc} = \frac{d \cos b \sin l}{R_{\rm pl}}.$$
$$\cos b_{\rm gc} = \frac{R_{\rm pl}}{d_{\rm gc}}.$$
$$\sin b_{\rm gc} = \frac{d \sin b}{d_{\rm gc}}.$$

where $R_{\rm pl} = \sqrt{R_\odot^2 + d^2 \cos^2 b - 2 \cdot R_\odot \cdot d \cos b \cos l}$ is the distance projected on the Galactic plane (see Figure 6.3, Moyano 2007), for a heliocentric distance d and Galactic coordinates (l, b). $R_\odot$ is the Solar Galactocentric distance.

To calculate all spatial velocities and rotation corrections, we used an ad hoc code developed by one of the authors (M.H.P.). This program yields results consistent with an independent software developed by S. Piatek (2005, private communication). All calculations were carried out using the heliocentric distances for the LMC/SMC given in Sections 4.1 and 4.2, a distance of 8.5 kpc from the Sun to the Galactic center, and the circular velocity of the LSR and peculiar velocity of the Sun relative to the LSR given above.

Table 9
Galactocentric Velocity Components of the LMC

Source	$V_{\rm gc,r}$	$V_{\rm gc,t}$
	(km s^{-1})	(km s^{-1})
Kroupa & Bastian 1997	+72 ± 52	+334 ± 52
K06b	+89 ± 4	+367 ± 18
PCM06 ($V_{\rm rot} = 50$ km s^{-1})	+80 ± 23	+347 ± 27
PI08	+93.2 ± 3.7	+346 ± 8.5
This work ($V_{\rm rot} = 50$ km s^{-1})	+86 ± 17	+315 ± 20
This work ($V_{\rm rot} = 120$ km s^{-1})	+94 ± 17	+280 ± 24

Table 10
Galactocentric Velocity Components of the SMC

Source	$V_{\rm gc,r}$	$V_{\rm gc,t}$
	(km s^{-1})	(km s^{-1})
Kroupa & Bastian 1997	+9 ± 177	+226 ± 177
K06a	+23 ± 7	+301 ± 52
PI08	+6.8 ± 2.4	+259 ± 17
This work	+20 ± 44	+258 ± 50

In Section 4.1, we presented two values for the CM proper motion of the LMC based on the two extreme values currently available for the rotational velocity of the plane of the LMC: 50 km s^{-1} (vDM02), and 120 km s^{-1} (PI08). For these two values, we obtain

$$V_{\rm gc,r} = +85.9 \pm 16.9 \, {\rm km \, s}^{-1}$$
$$V_{\rm gc,t} = +314.7 \pm 20.4 \, {\rm km \, s}^{-1} (V_{\rm rot,LMC} = 50 \, {\rm km \, s}^{-1}$$

and

$$V_{\rm gc,r} = +93.9 \pm 16.9 \, {\rm km \, s}^{-1}$$
$$V_{\rm gc,t} = +280.4 \pm 23.6 \, {\rm km \, s}^{-1} (V_{\rm rot,LMC} = 120 \, {\rm km \, s}^{-1})$$

for the gc velocity components of the LMC.

From the CM proper motion of the SMC given in Section 4.2, we obtain ($V_{\rm rot}$)

$$V_{\rm gc,r} = +19.6 \pm 44.0 \, {\rm km \, s}^{-1}$$
$$V_{\rm gc,t} = +257.6 \pm 49.9 \, {\rm km \, s}^{-1}$$

for the gc velocity components of the SMC.

In Tables 9 and 10, we compare our gc radial and tangential velocities for the LMC and SMC with previous results. Within the declared uncertainties, for the LMC there is a good agreement between previous results and our $V_{\rm gc,r}$; both for $V_{\rm rot,LMC}$ = 50 km s^{-1} and $V_{\rm rot,LMC}$ = 120 km s^{-1}. In contrast, our $V_{\rm gc,t}$ is in fair agreement with previous work for $V_{\rm rot,LMC}$ = 50 km s^{-1}, and in poor agreement for $V_{\rm rot,LMC}$ = 120 km s^{-1}. In the case of the SMC, both $V_{\rm gc,r}$ and $V_{\rm gc,t}$ are consistent with previous results.

Tables 11–13 summarize all the proper motion and velocity information obtained throughout our procedure. Rows 1 and 2 give field proper motion components and rows 3–4 give the corresponding CM proper motion components, both in equatorial coordinates. Rows 5–8 give the corresponding proper motions relative to the Galactic Rest Frame in equatorial and galactic coordinates (see Equation (7)). Rows 9–11 give the Π, Θ, and Z components of the gc velocities, and rows 12 and 13 the radial and tangential gc velocities, respectively.

The relative velocity between the LMC and the SMC can be derived from the Π, Θ and Z components of the space

Table 11
Proper Motion and Space Velocity of the LMC ($V_{\rm rot} = 50$ km s^{-1})

Parameter	Field: Q0557−6713
$\mu_\alpha \cos \delta$, Field (mas yr^{-1})	1.95 ± 0.13
μ_δ, Field (mas yr^{-1})	0.43 ± 0.18
$\mu_\alpha \cos \delta$, CM (mas yr^{-1})	1.82 ± 0.13
μ_δ, CM (mas yr^{-1})	0.39 ± 0.15
$\mu_\alpha^{\rm grf} \cos \delta$ (mas yr^{-1})	1.3 ± 0.1
$\mu_\delta^{\rm grf}$ (mas yr^{-1})	0.3 ± 0.2
$\mu_l^{\rm grf} \cos b$ (mas yr^{-1})	−0.5 ± 0.2
$\mu_b^{\rm grf}$ (mas yr^{-1})	1.3 ± 0.1
Π, velocity component (km s^{-1})	70 ± 38
Θ, velocity component (km s^{-1})	−238 ± 19
Z, velocity component (km s^{-1})	212 ± 19
$V_{\rm gc,r}$, radial velocity (km s^{-1})	86 ± 17
$V_{\rm gc,t}$, transverse velocity (km s^{-1})	315 ± 20

Table 12
Proper Motion and Space Velocity of the LMC ($V_{\rm rot} = 120$ km s^{-1})

Parameter	Field: Q0557−6713
$\mu_\alpha \cos \delta$, Field (mas yr^{-1})	1.95 ± 0.13
μ_δ, Field (mas yr^{-1})	0.43 ± 0.18
$\mu_\alpha \cos \delta$, CM (mas yr^{-1})	1.61 ± 0.13
μ_δ, CM (mas yr^{-1})	0.60 ± 0.15
$\mu_\alpha^{\rm grf} \cos \delta$ (mas yr^{-1})	1.1 ± 0.1
$\mu_\delta^{\rm grf}$ (mas yr^{-1})	0.5 ± 0.2
$\mu_l^{\rm grf} \cos b$ (mas yr^{-1})	−0.6 ± 0.2
$\mu_b^{\rm grf}$ (mas yr^{-1})	1.0 ± 0.1
Π, velocity component (km s^{-1})	116 ± 39
Θ, velocity component (km s^{-1})	−216 ± 19
Z, velocity component (km s^{-1})	165 ± 19
$V_{\rm gc,r}$, radial velocity (km s^{-1})	94 ± 17
$V_{\rm gc,t}$, transverse velocity (km s^{-1})	280 ± 24

Table 13
Proper Motion and Space Velocity of the SMC

Parameter	Field: Q0036−7227
$\mu_\alpha \cos \delta$, Field (mas yr^{-1})	0.95 ± 0.29
μ_δ, Field (mas yr^{-1})	−1.14 ± 0.18
$\mu_\alpha \cos \delta$, CM (mas yr^{-1})	1.03 ± 0.29
μ_δ, CM (mas yr^{-1})	−1.09 ± 0.18
$\mu_\alpha^{\rm grf} \cos \delta$ (mas yr^{-1})	0.6 ± 0.2
$\mu_\delta^{\rm grf}$ (mas yr^{-1})	−0.7 ± 0.2
$\mu_l^{\rm grf} \cos b$ (mas yr^{-1})	−0.6 ± 0.2
$\mu_b^{\rm grf}$ (mas yr^{-1})	0.7 ± 0.2
Π, velocity component (km s^{-1})	−63 ± 55
Θ, velocity component (km s^{-1})	−213 ± 50
Z, velocity component (km s^{-1})	132 ± 46
$V_{\rm gc,r}$, radial velocity (km s^{-1})	20 ± 44
$V_{\rm gc,t}$, transverse velocity (km s^{-1})	258 ± 50

velocities presented in Tables 11–13. They turn out to be 84 ± 50 km s^{-1}, for $V_{\rm rot,LMC}$ = 50 km s^{-1}, and 62 ± 63 km s^{-1} for $V_{\rm rot,LMC}$ = 120 km s^{-1}. Both results are consistent with the relative velocities given in K06a: 105 ± 42 km s^{-1} and PI08: 142 ± 19 km s^{-1}. Our high internal errors prevent strong conclusions about the gravitational binding of the MCs, but to illustrate we note that simple point-mass models indicate that for $M_{\rm LMC} \sim 2 \times 10^{10} \mathcal{M}_\odot$ (Schommer et al. 1992), the escape velocity of the SMC from the SMC is $\sim$90 km s^{-1}

($2 \times 10^{10} \mathcal{M}_\odot$ is a conservative value adopted in most numerical studies; see, e.g., GN96). In this oversimplified scenario, and albeit our large errors, our relative velocities are not inconsistent with the standard assumption that the MCs are gravitationally bound to each other.

Recent models by K06a, based on the theoretical platform originally developed by Murai & Fujimoto (1980), but using the data presented in K06a and K06b, are consistent with both bound and unbound orbits. A comparison of the total velocity of the LMC implied by our present-day velocities with that used in the models of K06a gives a difference of 53 ± 26 km s^{-1} for $V_{\rm rot,LMC} = 50$ km s^{-1}, and of 106 ± 26 km s^{-1} for $V_{\rm rot,LMC} = 120$ km s^{-1}. The same comparison yields a difference of 45 ± 67 km s^{-1} for the SMC. Within the declared uncertainties, there is a good agreement between our values for the SMC and those used in the models of K06a, but the agreement for the LMC is only fair for $V_{\rm rot,LMC} = 50$ km s^{-1}, and there is disagreement for $V_{\rm rot,LMC} = 120$ km s^{-1}.

Other notable models of the Magellanic system, including the MS, are those of GN96 and Heller & Rohlfs (1994, HR94). The first is a "Tidal Interaction" model, while the latter is a "Ram Pressure Stripping" model. A comparison of our present-day velocities for the MCs with those adopted for model calculations in GN96 gives differences in total velocity of 68 ± 39 km s^{-1}, LMC, $V_{\rm rot} = 50$ km s^{-1}, 115 ± 38 km s^{-1}, LMC, $V_{\rm rot} = 120$ km s^{-1}, and 114 ± 54 km s^{-1}, SMC. The corresponding comparison with HR94 gives: 79 ± 32 km s^{-1}, LMC, $V_{\rm rot} = 50$ km s^{-1}, 143 ± 31 km s^{-1}, LMC, $V_{\rm rot} = 120$ km s^{-1}, and 109 ± 49 km s^{-1}, SMC. Our value for the LMC and for $V_{\rm rot} = 120$ km s^{-1} is again discrepant, but there is a fair agreement in the case of the SMC, and for $V_{\rm rot,LMC} = 50$ km s^{-1}. Our results are slightly more consistent with GN96, marginally favoring the tidal interaction scenario to explain the formation of the MS.

7. THE MASS OF THE MILKY WAY

If we assume that all the mass of the MW is contained within the orbits of the MCs, and that the MCs have elliptical orbits around the Galaxy we can use the gc velocities derived in the previous section to estimate lower limits for the dynamical mass of our Galaxy, $M_{\rm Gal}$, through the expression for a point-like potential (Lin et al. 1995)

$$M_{\rm Gal} = \frac{R}{2\, G\, (1 - R/r_a)} \left(V_{\rm gc,r}^2 + V_{\rm gc,t}^2 \left(1 - \left(\frac{R}{r_a} \right)^2 \right) \right),$$

where r_a and R are the apogalacticon distance and the present gc distance, respectively.

Further assuming that the MCs are gravitationally bound to the Galaxy, demands in turn that r_a has to be less than our Galaxy's tidal radius with respect to M31 ($\sim$300 kpc; Lin et al. 1995).

From the LMC data, we obtain

$$M_{\rm Gal}(R < 50.1\,{\rm kpc}) = (7.3 \pm 0.9) \times 10^{11} \mathcal{M}_\odot$$
$$V_{\rm rot} = 50\,{\rm km\,s}^{-1})$$

and

$$M_{\rm Gal}(R < 50.1\,{\rm kpc}) = (6.0 \pm 0.9) \times 10^{11} \mathcal{M}_\odot$$
$$(V_{\rm rot} = 120\,{\rm km\,s}^{-1}).$$

The assumption that all of the MW is contained within the orbits of the MCs is quite strong (given the implications of

rotation curves of external galaxies; see, e.g., Lin et al. 1995; Rubin 1983), and it is possible that the Galactic Halo extends beyond the orbits of the MCs. In this context, the SMC could provide a better estimate of $M_{\rm Gal}$. From the SMC data, we obtain $M_{\rm Gal}\,(R < 61.7\,{\rm kpc}) = (5.8 \pm 2.2) \times 10^{11} \mathcal{M}_\odot$.

Our estimations of the lower limit of the dynamical mass of our Galaxy, turn out to be slightly larger than recent theoretical upper limits for its mass within 50 kpc given by Sakamoto et al. (2003): $\sim 5.5 \times 10^{11} \mathcal{M}_\odot$.

8. CONCLUSIONS

Here we summarize the main conclusions of this work.

1. We present the first results of a program to determine the proper motions of the LMC and SMC using QSOs in their background as reference points. Here we give final results for field Q0557$-$6713 in the LMC and field Q0036$-$7227 in the SMC. Although we went through the full reduction procedure for SMC field QJ0036$-$7225, it was impossible to use it to derive a reliable proper motion on account of unsolvable astrometric difficulties.

2. From field Q0557$-$6713, we have obtained a field proper motion of $\mu_\alpha \cos\delta = +1.95 \pm 0.13$ mas yr^{-1}; $\mu_\delta = +0.43 \pm 0.18$ mas yr^{-1} for the LMC.

3. From field Q0036$-$7227, we have obtained a field proper motion of $\mu_\alpha \cos\delta = +0.95 \pm 0.29$ mas yr^{-1}; $\mu_\delta = -1.14 \pm 0.18$ mas yr^{-1} for the SMC.

4. Applying perspective and rotation corrections to the field proper motion of the LMC, we derived its CM proper motion for two possible (extreme) values of its rotational velocity at the position of field Q0557$-$6713. We have obtained $\mu_\alpha \cos\delta = +1.82 \pm 0.13$ mas yr^{-1}; $\mu_\delta = +0.39 \pm 0.15$ mas yr^{-1}, for $V_{\rm rot} = 50$ km s^{-1}, and $\mu_\alpha \cos\delta = +1.61 \pm 0.13$ mas yr^{-1}; $\mu_\delta = +0.60 \pm 0.15$ mas yr^{-1}, for $V_{\rm rot} = 120$ km s^{-1}.

5. Assuming that the SMC has a disk-like central structure, and that it does not rotate, applying a perspective correction to its field proper motion leads to a CM proper motion of $\mu_\alpha \cos\delta = +1.03 \pm 0.29$ mas yr^{-1}; $\mu_\delta = -1.09 \pm 0.18$ mas yr^{-1} for the SMC.

6. Our field and CM proper motions are in reasonable agreement with most previous results, including recent HST measurements.

7. Complementing our proper motion data for the MCs with published radial velocities of their centers (LMC: +262.1 km s^{-1}, vDM02; SMC: +146.0 km s^{-1}, Harris & Zaritsky 2006 (+262.1 km s^{-1}, vDM02)) we derived their gc velocity components. For the LMC, we have obtained $V_{\rm gc,t} = +315 \pm 20$ km s^{-1}; $V_{\rm gc,r} = +86 \pm 17$ km s^{-1} ($V_{\rm rot} = 50$ km s^{-1}), and $V_{\rm gc,t} = +280 \pm 24$ km s^{-1}; $V_{\rm gc,r} = +94 \pm 17$ km s^{-1} ($V_{\rm rot} = 120$ km s^{-1}). For the SMC, we have obtained $V_{\rm gc,t} = +258 \pm 50$ km s^{-1}; $V_{\rm gc,r} = +20 \pm 44$ km s^{-1}.

8. These velocities imply a relative velocity between the LMC and SMC of 84 ± 50 km s^{-1} for $V_{\rm rot,LMC} = 50$ km s^{-1} and of 62 ± 63 km s^{-1} for $V_{\rm rot,LMC} = 120$ km s^{-1}. Albeit our large errors, these values are not inconsistent with the standard assumption that the MCs are gravitationally bound to each other.

9. Our results are slightly more consistent with the tidal scenario presented by GN96 to explain the formation of the MS.

REFERENCES

Anguita, C., Loyola, P., & Pedreros, M. H. 2000, AJ, 120, 845 (ALP00)
Arias, E. F., Charlot, P., Feissel, M., & Lestrade, J.-F. 1995, A&A, 303, 604
Baume, G., Carraro, G., Costa, E., Méndez, R. A., & Girardi, L. 2007, MNRAS, 375, 1077
Besla, G., Kallivayalil, N., Hernquist, L., Robertson, B., Cox, T. J., van der Marel, R. P., & Alcock, C. 2007, ApJ, 668, 949
Bevington, P. R. 1969, Data Reduction and Error Analysis for the Physical Sciences (New York: McGraw-Hill)
Blanco, V. M., & Heathcote, S. 1986, PASP, 98, 635
Carrera, R. 2006, PhD thesis, Univ. de la Laguna, Tenerife, Spain.
Carrera, R., Gallart, C., Aparicio, A., Costa, E., Méndez, R. A., & Noël, N. E. D. 2008, AJ, 136, 1039
Cioni, M.-R. L., van der Marel, R. P., Loup, C., & Habing, H. J. 2000, A&A, 359, 601
Connors, T. W., Kawata, D., & Gibson, B. K. 2006, MNRAS, 371, 108
Costa, E., & Loyola, P. 1999, A&AS, 139, 297
Cudworth, K. M., & Rees, R. F. 1991, PASP, 103, 470
Dehnen, W., & Binney, J. J. 1998, MNRAS, 298, 387
Drake, A. J., Cook, K. H., Alcock, C., Axelrod, T. S., & Geha, M (MACHO Collaboration) 2001, BAAS, 33, 1379
ESA 1997, VizieR Online Data Catalog, 1239, 0
Freedman, W. L., et al. 2001, ApJ, 553, 47
Gardiner, L. T., & Noguchi, M. 1996, MNRAS, 278, 191 (GN96)
Gardiner, L. T., Sawa, T., & Fujimoto, M. 1994, MNRAS, 266, 567
Gingold, R. A. 1984, PASA, 5, 469
Harris, J., & Zaritsky, D. 2006, AJ, 131, 2514
Heller, P., & Rohlfs, K. 1994, A&A, 291, 743 (HR94)
Irwin, M. 1999, IAU Symp. 192, The Stellar Content of Local Group Galaxies, ed. P. Whitelock & R. Cannon (San Francisco, CA: ASP), 409

Irwin, M. J., Demers, S., & Kunkel, W. E. 1996, BAAS, 28, 932
Jones, B. F., Klemola, A. R., & Lin, D. N. C. 1994, AJ, 107, 1333 (JKL94)
Kallivayalil, N., van der Marel, R. P., & Alcock, C. 2006a, ApJ, 652, 1213 (K06a)
Kallivayalil, N., van der Marel, R. P., Alcock, C., Axelrod, T., Cook, K. H., Drake, A. J., & Geha, M. 2006b, ApJ, 638, 772 (K06b)
Kroupa, P., & Bastian, U. 1997, New Astron., 2, 77
Kroupa, P., Röser, S., & Bastian, U. 1994, MNRAS, 266, 412
Lin, D. N. C., Jones, B. F., & Klemola, A. R. 1995, ApJ, 439, 652
Lynden-Bell, D., & Lynden-Bell, R. M. 1995, MNRAS, 275, 429
Mastropietro, C., Moore, B., Mayer, L., Wadsley, J., & Stadel, J. 2005, MNRAS, 363, 509
Mathewson, D. S., Wayte, S. R., Ford, V. L., & Ruan, K. 1987, PASA, 7, 19
Meurer, G. R., Bicknell, G. V., & Gingold, R. A. 1985, PASA, 6, 195
Momany, Y., & Zaggia, S. 2005, A&A, 437, 339 (MZ05)
Monet, D. G., Dahn, C. C., Vrba, F. J., Harris, H. C., Pier, J. R., Luginbuhl, C. B., & Ables, H. D. 1992, AJ, 103, 638
Moore, B., & Davis, M. 1994, MNRAS, 270, 209
Moyano, M. 2007, M.Sc. thesis, Univ. de Chile, Santiago, Chile.
Murai, T., & Fujimoto, M. 1980, PASJ, 32, 581
Noël, N. E. D., Gallart, C., Costa, E., & Méndez, R. A. 2007, AJ, 133, 2037
Olsen, K. A. G., & Massey, P. 2007, ApJ, 656, L61
Pedreros, M. H., Anguita, C., & Maza, J. 2002, AJ, 123, 1971 (PAM02)
Pedreros, M. H., Costa, E., & Méndez, R. A. 2006, AJ, 131, 1461 (PCM06)
Piatek, S., Pryor, C., Bristow, P., Olszewski, E. W., Harris, H. C., Mateo, M., Minniti, D., & Tinney, C. G. 2005, AJ, 130, 95
Piatek, S., Pryor, C., & Olszewski, E. W. 2008, AJ, 135, 1024 (PI08)
Röser, S., & Bastian, U. 1993, Bull. Inf. Cent. Donnees Astron. Strasbg., 42, 11
Rubin, V. C. 1983, Science, 220, 1339
Sakamoto, T., Chiba, M., & Beers, T. C. 2003, A&A, 397, 899
Schommer, R. A., Suntzeff, N. B., Olszewski, E. W., & Harris, H. C. 1992, AJ, 103, 447
Smart, W. M. 1977, Textbook on Spherical Astronomy (Cambridge: Cambridge Univ. Press)
Stanimirović, S., Staveley-Smith, L., & Jones, P. A. 2004, ApJ, 604, 176
Stetson, P. B. 1987, PASP, 99, 191
Tinney, C. G. 1999, MNRAS, 303, 565
Tinney, C. G., Da Costa, G. S., & Zinnecker, H. 1997, MNRAS, 285, 111
van der Marel, R. P., Alves, D. R., Hardy, E., & Suntzeff, N. B. 2002, AJ, 124, 2639 (vDM02)
van der Marel, R. P., & Cioni, M.-R. L. 2001, AJ, 122, 1807
Wayte, S. R. 1991, in IAU Symp. 148, The Magellanic Clouds, ed. R. Haynes, D. Milne (Dordrecht: Kluwer), 447
Yoshizawa, A. M., & Noguchi, M. 2003, MNRAS, 339, 1135
Zacharias, N., Urban, S. E., Zacharias, M. I., Wycoff, G. L., Hall, D. M., Monet, D. G., & Rafferty, T. J. 2004, AJ, 127, 3043
Zhao, H., Ibata, R. A., Lewis, G. F., & Irwin, M. J. 2003, VizieR Online Data Catalog, 733, 90701